Characterization of fractures in potential reservoir rocks for geothermal applications in the Rhine-Ruhr metropolitan area (Germany)

Martin Balcewicz[1,2], Benedikt Ahrens[3], Kevin Lippert[3,2], and Erik H. Saenger[1,3,2]

[1]Department of Civil and Environmental Engineering, Bochum University of Applied Sciences, Lennershofstraße 140, 44801 Bochum, Germany
[2]Institute of Geology, Mineralogy, and Geophysics, Ruhr-University Bochum, Universitätsstrasse 150, 44801 Bochum, Germany
[3]Fraunhofer IEG - Institution for Energy Infrastructures and Geothermal Energy, Lennershofstraße 140, 44801 Bochum, Germany

Correspondence: Martin Balcewicz (martin.balcewicz@hs-bochum.de)

Abstract. The importance of research into clean and renewable energy solutions has increased over the last decade. Geothermal energy provision is proven to meet both conditions. Therefore, conceptual models for deep geothermal applications were developed for different field sites regarding different local conditions. In Bavaria, Germany, geothermal applications were successfully carried out in carbonate horizons at depth of 4000 to $6000\,\mathrm{m}$. High permeability rates combined with sufficient thermal conductivities were mainly studied in karstified carbonates from the Late Jurassic reef facies. Similar to Bavaria, carbonates are located in the east of the Rhenohercynian Massif, in North Rhine-Westphalia (NRW), which quantification of the geothermal potential is still lacking. Compared to Bavaria, a supraregional carbonate mountain belt is exposed at the Remscheid-Altena anticline (NRW) from late Devonian and early Carboniferous times. The aim of our study was to examine the potential geothermal reservoir by field and laboratory investigations. Therefore, three representative outcrops in Wuppertal, Hagen Hohenlimburg, and Hönnetal were studied. During field surveys, 1068 discontinuities at various spatial scales were observed by scanline surveys. These discontinuities were characterized by trace length, true spacing, roughness, aperture, and filling materials. Joint orientation analysis indicated three dominant strike orientations in NNW−SSE, NW−SE, and NE−SW directions within the target horizon of interest. This compacted limestone layer (Massenkalk) is approximately $150\,\mathrm{m}$ thick and located at 4000 to $6000\,\mathrm{m}$ depth, dipping northwards at a dip angle of about 30 to $40°$. An extrapolation of the measured layer orientation and dip suggests that the carbonate reservoir extends below Essen, Bochum, and Dortmund. Our combined analysis of the field and laboratory results has shown that it could be a naturally fractured carbonate reservoir. We evaluated the potential fracture network in the reservoir and its orientation with respect to the prevailing maximum horizontal stress before concluding with implications for fluid flow: We proposed to focus on prominent discontinuities striking in NNW−SSE for upcoming geothermal applications, as these (1) are the most common, (2) strike in the direction of the main horizontal stress, (3) the fracture permeability significantly exceeds that of the reservoir rock matrix, and (4) because some of them are filled. Hence, the filled fractures bear the potential to be reopened by, for example, hydrochemical dissolution to create even better fluid efficiencies. Our results indicate that even higher permeability can be expected for karstified formations related to the

reef facies and hydrothermal processes. Our compiled data set consisting of laboratory and field measurements may provide a good basis for 3D subsurface modeling and numerical prediction of fluid flow in the naturally fractured carbonate reservoir. Further studies have to be elaborated to verify, if the fractured reservoir could possibly be reactivated by, for instance, hydraulic stimulation and thus enable geothermal applications.

1 Introduction

The Rhine-Ruhr metropolitan region in western Germany is one of the largest metropolitan areas in Europe. It has the largest European district heating network (AGFW, 2009) and is one of the largest energy systems in the world, which is predominantly fed by fossil fuels (Klaus et al., 2010). In recent decades, the Ruhr metropolitan area has been subject to structural changes associated with the ending of traditional coal mining and steel industry as well as accelerated urbanization. Considering effective climate changes, these processes pose local to global challenges for a post-fossil energy future. The polycentric structure of the Rhine-Ruhr area is particularly promising for the requirements imposed by the energy transition (Wegener et al., 2019). To account for the increasing demand for energy supply (e.g., Scheer et al., 2013; Araújo, 2014), the successful implementation of sustainable non-fossil energy concepts is required (e.g., geothermal energy; Fridleifsson et al., 2008; Goldstein et al., 2011). In recent years, many economically successful geothermal energy projects in Bavaria, southern Germany, have been realized and could serve as a valuable model for the Rhine-Ruhr area. The Bavarian part of the South German Molasse Basin has a high hydrothermal energy potential (Schellschmidt et al., 2010; Böhm et al., 2010; Stober, 2014; Homuth, 2014), which can be extracted from pre-existing fracture and karst systems in deep carbonate rocks (e.g., limestone deposits) of the Malm (Late Jurassic) formation (Fritzer et al., 2010). Similar to deep Bavarian deposits, carbonate rocks were accumulated in western Germany. Geothermal systems aiming for comparable geological carbonate horizons in the Rhine-Ruhr area are promising solutions to initiate the energy transition (Knutzen, 2017). The carbonates of the Rhine-Ruhr area were deposited extensively during Devonian times (Krebs, 1967; Koch, 1984; Koch-Früchtel and Früchtel, 1993). Today, those carbonates are exposed at the northern part of the Rhenohercynian Massif with thicknesses of approximately $150\,\mathrm{m}$ (Paeckelmann and Zimmermann, 1930; Paeckelmann, 1979; von Kamp and Ribbert, 2005). Based on limited exploration activities, these limestones are expected at depths relevant for deep geothermal applications (DEKORP Research Group, 1990). Younger, overburden sedimentary layers (Late Carboniferous) were deposited on top of the potential reservoir and the region became massively folded and faulted (Drozdzewski, 1985; Franke et al., 1990; Ziegler, 1990; Littke et al., 2008; Scheck-Wenderoth et al., 2008; Meschede, 2018). A feasibility study including extensive subsurface reservoir characterization and local geological site assessment is essential to describe the hydrothermal potential of presumably fractured and faulted carbonates in the Rhine-Ruhr area.

Determining the hydraulic, elastic, and thermal properties of a fractured carbonate reservoir is still associate with difficulties due to its accessibility, heterogeneity, and the in-situ conditions prevailing (i.e. stress and temperature). Even though very costly field measurements have been carried out, the characterization of the fractured reservoir is often complicated by insufficient field-based data, as they only provide a point by point insight into the reservoir properties (e.g., borehole logging; Da Prat, 1990). In addition, seismic surveys have been used for decades to indirectly estimate the properties and mechanical conditions

of fractured reservoirs (e.g., Far, 2011); although, the interpretation for complex, heterogeneous reservoirs is not unique. In the best case all field methods can be combined to reduce the geological ambiguity to characterize the reservoir in the best possible way. Since direct information on in-situ properties are limited and inaccessible (e.g., seismic tomography or well and borehole data), outcrop characterizations and laboratory measurements can provide the basis for reservoir characterization and the estimation of the potential reservoir behaviour under in-situ conditions.

The estimation and description of individual fractures and entire fracture networks in deep reservoirs is of elementary importance when it comes to reservoir characterisation. Fractures and fracture networks have a decisive influence on the fluid flow within the reservoir (e.g., Odling et al., 1999), but also on the stability (e.g., Cappa et al., 2005). They are typical observations at analogues outcrops and can be measured there (see review by Bonnet et al., 2001). While the origin of these typically tectonic driven fractures can be discussed extensively, the influence on reservoir permeability is obvious. Compared to the matrix permeability of the host rock, the permeability of fractures is generally several orders of magnitude higher (e.g., Nelson and Handin, 1977; Kranz et al., 1979; Evans et al., 1997; Ahrens et al., 2018). Detailed fracture analysis is essential to model reservoir quality, optimal well locations, and well performance (Nelson, 2001). Field surveys are both the first and one of the most crucial steps in the exploitation of the reservoir (van Golf-Racht, 1982; Agosta et al., 2010), that is, the investigation of the discrete fracture network (DFN). Furthermore, establishing correlations between outcrop and laboratory observations provide the basis for an improved analysis of seismic surveys, borehole logs, and fluid injection experiments to be performed.

In this integrated study, we examine the geothermal potential of deep carbonates in the Rhine-Ruhr area, by combining field and laboratory investigations of pre-existing fractures and fracture networks on outcrop and sample scale. The combined analysis of field and laboratory measurements allows us to describe the potential carbonate reservoir by characterizing its natural fractured systems. Three outcrop analogues on the eastern side of the northern Rhenohercynian Massif have been chosen for field survey and sample collection. All quaries are located within the Devonian Reef Complex and compacted limestone (Massenkalk) from Middle and Upper Devonian are the dominant stratigraphic units in those quarries (Krebs, 1970; Paeckelmann, 1979; Schudack, 1993). Dominant fracture systems and different facies have been documented and sampled. Most of these measurements have been conducted by one-dimensional scanline surveys (Priest and Hudson, 1976, 1981). Representative fresh rock samples have been taken directly from the outcrop wall. Porosities, ultrasonic velocities, dynamic elastic moduli, thermal properties, and permeabilites were determined by laboratory measurements.

In the following, we first introduce the geology of the Devonian Reef Complex. We proceed by describing the outcrops and the employed field and laboratory methods. Following the presentation of the measurements results, we conclude by discussing the geothermal potential of the geological subsurface model, that is, the deep carbonate layers and their fracture systems.

2 Geology, Outcrop Investigations, and Laboratory Measurements

2.1 Geological Setting: The Devonian Reef Complex

The Rhenohercynian Massif is the European most northern mountain belt, which was defined after Kossmat (1927). The massif is the result of a shallow marginal sea which was surrounded by Laurussia in the North (Old-Red Continent and Baltica) and

the micro-continent Avalonia in the South. During the Early Devonian, a passive continental margin evolved to the South of Laurussia which was affected by crustal thinning. On top of the thin crust a shelf sea derived called the Rhenohercynian basin. The flat sea from Bretagne, Belgium up to Germany was filled by clastic shelf deposits and carbonates derived from Laurussia. An overall tectonic NW-movement dominated during Hercynian Orogeny and lead to extensions, periodic trans-, and ingressions within the Rhenohercynian basin. In the late Middle Devonian, Avalonia moved northwards and the sedimentation in the offshore belt decreased. The ongoing NW-movement enhanced submarine volcanic mounds which favoured growth of carbonates and coral/stromatoporoid reefs on the shelf (Jux, 1960; Grabert, 1998; Dallmeyer et al., 2013; Franke et al., 2017). An elongated reef complex developed along Laurussia's coastline, the so-called the Devonian Reef Complex (Krebs, 1970). The Devonian Reef Complex can be traced over an area from the Neandertal-Valley (Düsseldorf) to Dornap, Wuppertal, Schwelm, Hagen Hohenlimburg, Letmathe, Sundwig, Iserlohn, Hemer to Balve (Fig. 1a). Furthermore, these horizons can be observed in boreholes in northern Germany (e.g., Hesemann, 1965, Münsterland 1). Continued crustal extension and subsidence are marked by a transition from siliciclastic, deltaic shallow-marine environments (Rhenish facies), to an open-marine shale and pure limestone dominated facies (Hercynian facies) (Krebs, 1970; Grabert, 1998; Pas et al., 2013; Meschede, 2018). Shelf clastics and carbonates are overlain by hemipelagic deposits (Dallmeyer et al., 2013). During Late Devonian and Early Carboniferous, the reef complex receded northwards and sedimentation changed while closing the Rhenohercynian basin. Primary caused by tilting blocks and faulting, first graywacke turbidites and secondly a quartz-rich sandstone were deposited in the foreland. Further, during Late Carboniferous sedimentation continued and resulted in interbedded sequences of the Ruhr coal district at the northwestern margin of the Rhenohercynian foreland. From Early Carboniferous onwards, the deposited sediments were compressed and folded by the Hercynian Orogeny. Simultaneously, the thick accumulations of sediments (3-12 km) were thrusted by reactivated listric normal faults during NW-movement (Oncken, 1997; Franke et al., 1990; Engel et al., 1983; Franke and Engel, 1982; Holder and Leversidge, 1986; Meschede, 2018). Between Early Triassic and Late Cretaceous at least two more extension sequences arose and caused NE-SW-directed shortening (Brix et al., 1988; Drozdzewski and Wrede, 1994). Since Eocene, the complex tectonic setting is affected by a further extensional regime (Kley, 2013).

2.2 Study Areas

Three stone pits have been chosen for field studies within the Devonian Reef Complex: (1) stone pit Osterholz located in Wuppertal, (2) quarry Oege in Hagen Hohenlimburg, and (3) quarry Asbeck in Hönnetal (Fig. 1a). The outcrops in Osterholz, Oege, and Asbeck are active open pit mines and are driven by independent companies called Kalkwerke H. Oetelshofen GmbH & Co. KG, Hohenlimburger Kalkwerke GmbH, and Rheinkalk GmbH, respectively. The entrances of the three quarries are located at (1) E ^{36}3372, N ^{56}79249, (2) E ^{40}1215, N ^{56}89459, and (3) E ^{40}0334, N ^{56}93287 (Fig. 3). In the following the outcrops will be referred according to their geographical location: Wuppertal (WOH), Hagen Hohenlimburg (HKW), and Hönnetal (HLO).

The quarry Osterholz in Wuppertal is located in the Osterholz graben which is limited by the Herzkamper syncline to the North and the Wupper river to the South (Fig. 1a). The regional geology is dominated by WSW−ENE striking folds which are associated with the Hercynian orogeny (Paeckelmann, 1979). The Herzkamper special syncline can be understood as an

extension of the most-southern syncline in the foreland basin (Wittener syncline, Ruhr-Coal-District) but should be considered as an individual syncline separating the Remscheid-Altena anticline, in the South, from the Velbert anticline, in the North (Paeckelmann, 1979). The compacted limestone deposits (Massenkalk) are located in an approx. $10\,\mathrm{km}$ long graben which strikes parallel to the Hercynian induced folds. This thrusted graben results into numerous smaller horses. The tectonic regime of this system was mainly affected by the Hercynian orogeny and became further compressed by recent folding processes in the South. The stratigraphic unit of the quarry Osterholz in Wuppertal is Upper Givetian (approx. 382 Ma), primarily the Schwelm facies (according to Krebs, 1970). The studied limestone layers with a mean thickness of 1 to 5 m showed grayish, compacted layers of well-bedded carbonates with corals, stromatoporoidea, and bioclastic materials. This approximately 150 m thick horizon sits on top of dolomitic carbonates and is either related to the brachiopoda- and coral rich series of stromatopora series. The limestone bed boundaries show mechanical and fracture stratigraphy. Both series are indicators for the closer back-reef lagoon facies (Krebs, 1967; Koch, 1984; Grabert, 1998; Paeckelmann, 1979). However, dolomitic blocks also occurred in a small number.

The regional tectonic setting in Hagen Hohenlimburg was massively affected by the Remscheider anticline, the Ennepe-Thrust, and the Großholthausener fault (Fig. 1a). In the South of Hagen Hohenlimburg several smaller scaled anticlines occur with lengths of 100 to $1000\,\mathrm{m}$. These anticlines follow the Hercynian general striking direction of WSW−ENE and plunge steep to the North with an angle of about $25°$. Within these anticlines, smaller special folds are documented (von Kamp and Ribbert, 2005). In the northern limb of the Remscheider anticline, where the studied quarry was set, the Hasper anticline and Voerder syncline can be found. Both folds are monoclines and their steep limbs rapidly end when intersecting the regional normal fault Großholthausener fault. In the East of the Großholthausener fault, the quarry Oege in Hagen Hohenlimburg can be found. The quarry is surrounded by the river Lenne and some smaller normal faults. In the North, the devonian carbonate layers are cut by the Ennepe-Thrust. Krebs (1970), Flügel and Hötzl (1976) and Koch-Früchtel and Früchtel (1993) characterized the local compacted limestone in the quarry Oege as Schwelm facies. The quarry is enriched in dolomite due to hydrothermal veins (von Kamp and Ribbert, 2005). These dolomitic carbonates manifest in a high degree of fractured blocks and karst formations which were filled by tertiary- and cretaceous-sediments, respectively. The carbonates, which were untouched by the hydrothermal veins, contain brachiopoda, bivalves, crinoids, corals, gastropoda, stromatoporoidae, and micrite. These carbonates are identified as Middle Devonian (Givetian according to Basse et al., 2016). The compacted limestone was mapped as irregular, lens shaped coral reefs (von Kamp and Ribbert, 2005). Those small reefs have been characterized as a preliminary stage of the today known Devonian Reef Complex. The complex distribution in the subsurface is still heavily debated (e.g., Salamon and Königshof, 2010). A detailed profile was taken by Koch-Früchtel and Früchtel (1993) and reveals compacted limestone with numerous dolomitic carbonate layers (mean thickness $20\,\mathrm{m}$). Below the Schwelm facies, layers of carbonatic siltstones and claystones, called the Oege Beds (Upper Honsel Beds), are located. Furthermore, a full-microfacies analysis was made by Koch-Früchtel and Früchtel (1993) and subdivides the Schwelm facies into shallow to open sea lagoons which are affected by sea current.

The quarry Asbeck in Hönnetal is located to the North of the Remscheid-Altena anticline (Fig. 1a). Due to its special location, the northern limb of the anticline, the geological regime can be described as a very basic setting. The exposed compacted

limestone deposits are dipping gently to the north and are surrounded by older Devonian sediments in the South and early Devonian, late Carboniferous sediments to the North. The regional setting is dominated by NNW−SSE striking strike-slip faults which are associated to the folding mechanics during Hercynian orogeny (Paeckelmann, 1938). Those strike-slip faults can be tracked along the major Remscheid-Altena anticline structure. At the most eastern part of the Remscheid-Altena anticline, the tip of the fold is plunging to the NNE direction. This affects the mentioned strike-slip faults which results into some bent fault formations along the plunged tip of the anticline. During folding, weak bedding planes became thrusted and became reactivated during later tectonic events. The local stratigraphy of the quarry Asbeck in Hönnetal consists of an initial bank stadium (Schwelm Facies) that developed into a true bioherm complex, that is, Dorp Facies (Becker et al., 2016). Schudack (1993) has investigated the different facies and cyclic depositions of the reef and back-reef lagoon facies and subdivided these facies into six subfacies which were investigated in more detail by Kloke (2007). The grayish, highly compacted limestones (approx. $600\,\mathrm{m}$ thickness) containing corals, stromatoporoidea and Brachiopoda are associated with late Middle Devonian (Givetian) or early Late Devonian (Frasnian). Except some minor parts, that were mentioned by Kloke (2007), no dolomitic rocks were documented.

The selected quarries show similar bedding planes with comparable dip directions. In the quarries Wuppertal, Hagen Hohemlimburg and Hönnetal, mean bedding is approximately $327°$, $345°$, and $18°$ in dip direction with a dip angle of about 30 to $45°$, $42°$, and $28°$ in respect to dip direction, respectively. The working levels of each stone pit were approximately oriented perpendicular to each other and strike NNW−SSE and NE−SW (Fig. 3).

2.3 Field Method: Outcrop Scanline Surveys

The term discontinuity and its origin can be looked up in many textbooks on structural and engineering geology (e.g., Priest, 1995). In the following, we define a discontinuity as a weak zone within a rock mass that can be referred to as a fracture, joint, vein or fault. Unlike the International Society for Rock Mechanics (ISRM, 1978), we neglect weak bedding planes or schistosity planes in the field surveys. Nevertheless, we distinguish between natural discontinuities, which are associated to geological origins, and artificial discontinuities which result from anthropogenic processes (e.g., drilling, blasting or excavation).

The discontinuities were recorded by a scanline sampling technique according to Priest and Hudson (1981). The advantages and disadvantages of this method have already been discussed in detail in several studies over the last decades (e.g., Attewell and Farmer, 1976; Priest and Hudson, 1981). Based on our field observations, we make the simplified assumption that spatially homogeneous fracture networks are dominant in the outcrops, whereby this depends on the spatial scale of observation. In regions with spatially heterogeneous fracture networks, however, more complex methods than the scanline sampling technique are required for fracture characterization (e.g., Watkins et al., 2015). According to the study of Priest and Hudson (1981), this paper focuses only on the most important parts of this technique. The setting of a scanline survey is a tape line, which is fixed firmly to the exposed rock wall and shows a start and an end point. The length of a scanline can range from a few decimetres to several metres. Estimates of all possible sources of error have shown that the number of measured and recorded discontinuities is more significant than the length of the scanline (Priest and Hudson, 1981). Hence, for each quarry we selected representative, safe rock walls where at least 30 measurable discontinuities (number of discontinuity observations $n \geq 30$) could be recorded.

After the tape line was fixed, the trend and plunge angle of the tape line were measured. The trend angle reflects the orientation of the tape line ($\alpha_{\mathrm{S}} = 0° \equiv$ North; $\alpha_{\mathrm{S}} = 180° \equiv$ South), which corresponds to the strike of the rock wall. The angle of plunge shows the levelling of the tape line (approx. $0° \leq \beta_{\mathrm{S}} \leq 15°$). After the tape line was installed, each discontinuity that intersected the tape line was recorded and categorized according to the following six properties (cf. Table 1):

1. **Intersecting distance:** The intersecting distance corresponds to the distance between each intersecting discontinuity and the fixed starting point of the tape line.

2. **Discontinuity length:** The installed tape line and the intersecting discontinuity meet at an intersecting point. The trace length above and below the tape towards the joint tips indicates the length of the discontinuity. If both tips exceed the rock walls height, the discontinuity is recorded as "through-going". Accordingly, discontinuities of which one or both ends are visible are categorized as "one end visible" or "both ends visible". On rare occasions, neither of both ends can be recorded, then the discontinuity is documented as "neither ends visible".

3. **Orientation:** The attitude of a discontinuity in space is called the orientation. The orientation is described by the dip direction (azimuth) and the dip of the line of the steepest declination in the plane of discontinuity.

4. **Roughness:** Roughness is the inherent alignment and waviness of the surface at the mean level of a discontinuity. A large-area waviness may also alter the dip locally. All roughness measurements were recorded manually. Therefore, we distinguish between smooth, slightly rough, and rough, both on mesoscopic and field scale. On the mesoscopic scale, the fracture surfaces were analysed for mineral steps, stylotites, or plumose structures. On the field scale, the fracture roughness was determined by wavelength measurements with a tape line.

5. **Aperture:** Aperture is the perpendicular distance between adjacent rock walls of a discontinuity where the space between them is filled with a material, that is, filling.

6. **Filling:** Filling is the material that separates the adjacent rock wall of a discontinuity and is usually weaker than the parent rock. In our study, typical filling materials are calcite, clay or debris. These includes thin mineral coatings and healed discontinuities such as quartz and calcite veins.

In spite of the above-mentioned records, it must be emphasized again how important the calculation of the intersecting angle is. Due to an irregular outcrop wall, the distance between the starting point and the recorded discontinuity (i.e. apparent spacing) is measured incorrectly. This apparent distance distorts the true orientation of the discontinuity. The true angle δ between the scanline orientation (trend/plunge) and the normal to the recorded discontinuity was calculated according to

$$\delta = \arccos(\cos(\alpha_{\mathrm{n}} - \alpha_{\mathrm{s}})\cos(\beta_{\mathrm{n}})\cos(\beta_{\mathrm{s}}) + \sin(\beta_{\mathrm{n}})\sin(\beta_{\mathrm{s}})), \tag{1}$$

where α_s, β_s, α_n, and β_n denote the trend direction of the tape line (scanline), the plunge direction of the tape line with regard to trend orientation, and the dip direction and dip of the normal to the fracture, respectively. Further, the true angle δ and the

apparent spacing χ_s between two discontinuities were used to calculate the true spacing assuming a homogeneous fracture pattern $\chi_r = \cos(\delta)\chi_s$. By evaluating the ratio of true discontinuity spacing χ_r and the number of discontinuity observations the mean discontinuity spacing $\bar{\chi} = \lambda^{-1} = (\sum \chi_r)n^{-1}$ was determined, where λ denotes the discontinuity frequency. The evaluation of the mean discontinuity track length with respect to the required accuracy has already been discussed in detail by Priest and Hudson (1981). The authors have made various suggestions when the end of a discontinuity trace on an investigated rock wall may not be visible, for example, due to geological events or anthropogenic processes. In our study, the proposed solution for censored semi-trace length sampling was adopted to evaluate the mean discontinuity track length μ_i. If the distribution of trace length over the recorded rock wall follows a power-law distribution, then the frequency $f(l)$ is given by $f(l) = \lambda e^{-\lambda \bar{\chi}}$. Following the approach of Priest and Hudson (1981), for censored semi-trace length analysis the mean discontinuity trace length was determined according to

$$\mu_i{}^{-1} = \mu^{-1} - (ce^{-\mu c})(1 - e^{-\mu c})^{-1}, \tag{2}$$

where μ and c denote mean population frequency and concealed trace length of the recorded discontinuity, respectively. Typically, the concealed trace length is one order of magnitude smaller than the recorded trace length. Note that discontinuities exceeding the height of the outcrop wall could be detected at the nearest level above and/or below the quarry. In addition, the simplified 2D fracture connectivity of fractures aligned perpendicular to the examined outcrop face, that is, the average number of discontinuity intersections per discontinuity P, was estimated for each opencast mine according to Ozkaya (2011)

$$P = \sum_{k}^{n} d_k{}^{-1} \sum_{k}^{n} d_k \sum_{j \neq k}^{n} d_j \, L_j \sin(\Delta\theta_{jk}), \tag{3}$$

where $\Delta\theta_{jk}$, d_j, and L_j denote the angle between the average striking directions of two discontinuity sets j and k, the number of discontinuities per total scanline length (i.e., fracture density), and the mean discontinuity length of each discontinuity set, respectively. In each outcrop we encountered three sets of fractures ($n = 3$) in the respective investigated carbonate layers. Therefore, the average fracture connectivity P of each exposed carbonate layer was estimated on the basis of three average fracture densities and mean discontinuity lengths.

The recorded discontinuities were evaluated with MATLAB (2018) after Hudson (2005) and Markovaara-Koivisto and Laine (2012). Markovaara-Koivisto and Laine (2012) developed an open source MATLAB code for the visualization of scanline survey results that was adapted to the purpose of this study. All measurements were recorded according to the metric system of measurement.

2.4 Laboratory Measurements: Petrophysical Characterization of Samples

During the field work, loose rock blocks were taken in each quarry for further petrophysical characterization. Compacted limestones, dolomites, and red, dolimitc rocks were named MKB (black Massenkalk), MKY (yellow Massenkalk), and MKR (red Massenkalk), respectively. After sampling the rocks were named according to the sampled quarry, sampled working level, rock type, and sample number. Representative, cylindrical cores with a diameter of $40\,\mathrm{mm}$ were extracted from each of

these blocks by diamond core drilling perpendicular to the bedding direction. In addition, it was possible for one rock sample (HKW-2-MKB-2-S2) to be cored directly at an exposed rock wall in the outcrop of Hagen Hohenlimburg with a mobile drilling machine. All samples, whether cored in the laboratory or the outcrop, were saw-cut plane-parallel and their end faces were ground square to the maximal possible length l (Table 4). A diameter-to-length ratio of 1:2.5 was aimed for, but this could not always be achieved due to the high density of pre-existing fractures in some blocks. This target sample geometry is generally recommended for triaxial deformation experiments on cylindrical samples (Paterson and Wong, 2005), a topic that exceeds the scope of our current study. All steps of the preparation were conducted with water as coolant and for rinsing removed material. Following preparation, samples were oven-dried at $60\,^{\circ}\mathrm{C}$ for about $48\,\mathrm{h}$. Basic petrophysical properties were determined on identically prepared samples at ambient conditions, except permeability, which was derived under elevated pressures.

Bulk density ρ_{geo} was calculated from the geometrical volume of the cylindrical samples and their dry masses. Grain density ρ_{grain} was gained from pycnometer measurements on rock powder, produced by crushing and grinding of leftover rock fragments, in compliance with the German DIN 18124 standard. By evaluating the ratio between bulk and grain density, the total porosity was determined according to $\phi_{\mathrm{tot}} = 1 - (\rho_{\mathrm{geo}}/\rho_{\mathrm{grain}})$. The connected porosity, that is, the externally accessible and connected pore volume, was determined using the difference of the masses of dry and saturated samples with distilled water (see Duda and Renner, 2013).

Ultrasonic P- and S-wave velocities, v_{P} and v_{S}, were determined on dry and saturated samples from first-arrival measurements using an ultrasound benchtop unit composed of a waveform generator, two identical broadband ultrasound sensors ($1\,\mathrm{MHz}$ centre frequency and $0.5\,\mathrm{in}$ diameter), and a digital storage oscilloscope ($200\,\mathrm{MHz}$ sampling frequency). Measurements were performed parallel to the cylinder axis, that is, the drilling direction. Velocities were calculated by dividing the sample length by the determined arrival times less the travel time in the assembly parts. Drained dynamic Young's modulus $\tilde{E}_{\mathrm{d}}$ and Poisson's ratio $\tilde{\nu}_{\mathrm{d}}$ were calculated by dry P- and S-wave velocities, $v_{\mathrm{P,dry}}$ and $v_{\mathrm{S,dry}}$, and bulk density assuming isotropy (see Mavko et al., 2020). Moreover, saturated P- and S-wave velocity, $v_{\mathrm{P,sat}}$ and $v_{\mathrm{S,sat}}$, and the density of the fluid-saturated sample was used to calculate undrained Poisson's ratio $\tilde{\nu}_{\mathrm{ud}}$ and Young's modulus $\tilde{E}_{\mathrm{ud}}$, assuming isotropy and employing Gassmann's hypothesis (Gassmann, 1951) that S-wave velocity remains unaffected by the presence of a fluid ($v_{\mathrm{S,dry}} = v_{\mathrm{S,sat}}$).

Thermal conductivity κ_{dry} of the dry sample cores was determined by a thermal conductivity scanner using an optical-scanning-method at ambient conditions (Popov, 1997). The scanner consists of an emitter and a measuring unit, that is moved along the sample at a fixed distance. The emitted light and heat radiation is focused on the surface of the sample, which heats up the sample pointwise. To ensure absolute absorption of the energy, a part of the sample, usually a strip, was painted black. Furthermore, it was ensured that the samples for thermal conductivity measurements meet the geometrical requirements for sample size in order to reduce boundary effects. Infrared temperature sensors are located at a fixed distance from the emitter (lead sulfide infrared receiver) and measure the temperature difference of the sample before and after heating. The thermal conductivity was determined by comparison with known standards. In this study, we used the standards of quartz (κ_{qtz} = $1.35\,\mathrm{W(mK)^{-1}}$) and titanium alloy ($\kappa_{\mathrm{Ti}}$ = $6.05\,\mathrm{W(mK)^{-1}}$). According to the manufacturer (Lippmann and Rauen GbR; TCS No. 2010-013), the determination of thermal conductivity is subject to an absolute error of approximately $3\,\%$.

Permeability k of the samples were determined using Darcy's Law (Darcy, 1856) and a conventional Hoek cell (Hoek and Brown, 1997) to apply axial load, pore-fluid pressure, and confining pressure. Axial pistons and the pre-saturated samples were jacketed by a rubber tube to prevent oil from penetrating the sample, that is, a connection between confining and pore pressure. In addition, confining and pore-fluid pressure were kept below the axial pressure. A hand pump was operated supplying the axial load ($12\,\mathrm{MPa}$). A computer-controlled, high-pressure metering pump was used to apply confining pressure on the sample by compressing distilled water ($10\,\mathrm{MPa}$). Axial pore-fluid flow was ensured through central bores in the axial loading pistons. Distilled water was pumped from a water reservoir through the lower end face of the samples either by applying constant flow rates (0.001 to $0.15\,\mathrm{l\,h^{-1}}$) by a second, identical metering pump. The lower axial loading piston was equipped with an outlet pipe discharging fluid pressure to atmosphere (i.e. $1\,\mathrm{bar}$). The temperature and pressure of the pore-fluid was measured to calculate the temperature- and pressure-dependent fluid viscosity according to Wagner (2009). Only permeability of the naturally fractured dolimite sample (HKW-2-MKB-2-S2) was investigated at three different stress stages. Each permeability of the samples indicated below corresponds to the arithmetic mean value of all experiments conducted with various flow rates for conditions of steady-state fluid flow.

3 Results

In the following, the general findings from the field discontinuity investigations, which are found in all outcrops, are presented first, before each outcrop is described individually. Then, the results of the laboratory investigations are introduced. Furthermore, descriptive links between both field and laboratory results are established.

3.1 Field Discontinuity Observations

A total of 1068 discontinuity observations were recorded and classified (e.g., discontinuity type, filling, and roughness) by using the field surveys in the three outcrops in Wuppertal, Hagen Hohenlimburg, and Hönnetal (Table 2). It was found that essentially three main sets of discontinuity orientations are predominant in all outcrops (Table 3). In Wuppertal the sets are grouped into the directions NNW−SSE, NE−SW, and NW−SE (Fig. 4c,d). In contrast, the discontinuity sets in Hagen Hohenlimburg and Hönnetal are oriented towards NNE−SSW, NW−SE and ENE−WSW, and N−S, W−E and ENE−WSW, respectively (Figs. 5c,d; 6c,d). The dip angles of the discontinuities were documented very steep, that is, between $80°$ and $90°$ (dip) in all three quarries. By further differentiating the strike directions of the classified discontinuity sets further according to their filling material differences between calcite and debris-filled fractures can be identified (Fig. 7). Our data tend to show a slight strike rotation between paleo-filled and debris-filled discontinuities in NNW−SSE direction.

"Wuppertal". During the field observations in Wuppertal, scanline surveys were taken in two orientations NNW−SSE and NE−SW. Eight scanline surveys were measured with a total length of $66.6\,\mathrm{m}$ and 461 discontinuity measurements were performed (Table 3). We recorded steep dip angles for all joint orientations (Fig. 4). More than 130 measurements could be assigned to each of the three main discontinuity sets. Orientations of 257/88, 145/82, and 017/89 (dipdir/dip) were determined for the these three sets. A total of 59 discontinuities were recorded as open fractures, 87 as closed fractures, 270 as filled

fractures and 45 with slickensides along the fracture plane. Among the 270 filled fractures, 116 were identified with calcite and 154 with recent debris. No significant difference in the strike direction of the paleo and debris-filled discontinuities can be detected (Fig. 7a,b). The average paleo-filled and debris-filled fracture strike directions are 177°and 178°, respectively. Four discontinuities exceeded the height of the rock face, both ends were visible in 356 recordings, one end was recorded in 93 discontinuities, and in eight joints neither end was visible. The roughness recordings on field scale showed 354 smooth surfaces, 81 fractures were slightly rough and 26 fractures were recorded as rough. On mesoscopic scale, 159, 250, and 52 joints were recorded as smooth, slightly rough, and rough, respectively. The mean discontinuity trace length and mean discontinuity spacing are $6.65\,\mathrm{m}$ and $0.15\,\mathrm{m}$, respectively (Fig. 4a,b). The 461 recorded discontinuities can be divided into three sets according to their orientations (Fig. 4b), whereby set 1, 2, and 3 could be assigned 181, 142, and 138 discontinuities, respectively. On average 2.71, 2.13, and 2.07 discontinuities or fractures were recorded per scanline meter in the sets 1, 2, and 3, respectively, corresponding to the average fracture density of the corresponding sets. For the sets 1, 2 and 3 the average discontinuity lengths amount to 7.01, 4.07 and $11.43\,\mathrm{m}$, respectively. The angles between the average striking direction of set 1 and 2, set 1 and 3, and set 2 and 3 were derived as 112°, 62°and 50°, respectively. This results in an average number of discontinuity intersections per discontinuity of 21.42, that is, the estimated 2D fracture connectivity according to Ozkaya (2011). The identified fracture interconnection in this outcrop is about 6 to 8 times higher than in the other outcrops Hönnetal and Hagen Hohenlimburg.

"Hagen Hohenlimburg". In Hagen Hohenlimburg the scanline surveys were conducted on two exposed rock walls with the orientations NNW−SSE and ENE−WSW. Over a total length of $76.15\,\mathrm{m}$ 361 discontinuities were recorded, which were divided into three sets of main orientations (Table 2). The set 1 lists 134 discontinuity observations, that show a mean common orientation of 224/89 (dipdir/dip) (Table 3). Sets 2 and 3 comprise 95 and 132 discontinuities with an average orientation of 282/84 and 345/80 (dipdir/dip), respectively. The discontinuities recorded here show a varying angle of dip and no clear predominant dip and direction (Fig. 5). Of the 361 recorded discontinuities, 26 could be classified as open, 40 as closed, 258 as filled and 37 as slickenside discontinuities. Calcite is listed as the dominant filling material with 160 entries, recent debris was recorded in 98 observations within the fractures. Here, the disagreement between the average calcite-filled fracture strike direction and that with debris becomes more apparent (Fig. 7c,d). The average paleo-filled and debris-filled fracture strike directions are 135° and 154°, respectively. 20 discontinuities exceeded the height of the rock wall, in 300 recordings both ends were visible, one visible end was documented for 37 cases, and neither end was registered in four joints. The roughness of 194 discontinuities was classified as smooth, 116 as slightly rough and 51 as rough on the field scale. On the mesoscopic scale 77 smooth, 184 slightly rough and 100 rough discontinuities were observed. The mean joint track length and the mean joint distance differ significantly from the measurement results from the other quarries and amount to $1.23\,\mathrm{m}$ and $0.24\,\mathrm{m}$, respectively (Fig. 5a,b). The discontinuities recorded in this outcrop show three different strike directions (Fig. 5b) and were therefore divided into three sets with 134, 95, and 132 discontinuities. The fracture densities of set 1 to 3 were calculated as 1.76, 1.25, and $1.24\,\mathrm{m}^{-1}$, respectively. The mean discontinuity length of the discontinuity set 1, 2, and 3 amounts to 1.24, 0.96, and $1.46\,\mathrm{m}$, respectively. The discontinuity lengths determined here are the smallest of all recorded discontinuity sets of all quarries. The average strike difference direction between the sets $\theta_{1,2}$, $\theta_{2,3}$, and $\theta_{1,3}$ were calculate as 122°, 63°, and 59°,

respectively. The value of fracture connectivity P determined for Hagen Hohenlimburg is 2.49 and corresponds to the smallest value of all examined quarries.

"Hönnetal". In Hönnteal 246 discontinuities were recorded on two rock faces, which are oriented in the direction NNW−SSE and ENE−WSW. All in all $62.76\,\mathrm{m}$ of scanline surveys were recorded and three sets of predominant orientations have been identified (Table 2). The number of observations for each set was recorded at 82, 24, and 140, and the dominant orientations for each set were derived at 266/75, 331/79, and 359/87 (dipdir/dip) (Fig. 6). 21 of 246 observations were made for open discontinuities, 34 for closed, 188 for filled, and three fractures showed slickensides on their fracture surfaces. Calcite was discovered as the dominant filling material with 137 records and 51 showed debris deposits. The difference between the striking of calcite and debris-filled fractures is about 34° (Fig. 7e,f). The height of the rock face was exceeded by 29 discontinuities, both ends were visible in 116 joints, one end was found in 96 joints, and in five joints neither end was visible. On a field scale, the majority of the fracture surfaces were classified as smooth (216), whereas the number of slightly rough (26) and rough fracture surfaces (four) is relatively small. In contrast, on a mesoscopic scale, 55, 155, and 36 discontinuities were found to have smooth, slightly rough, or rough fracture surfaces, respectively. The mean discontinuity trace length was determined to be 3.94 m and lies between the mean trace lengths of the other two outcrops. The mean discontinuity distance is similar to the one determined during the surveyed discontinuities in Hagen Hohenlimburg and was determined to be $0.27\,\mathrm{m}$. In Hönnetal, too, the over 200 recorded discontinuities occur in three clusters or sets of striking directions. The sets 1 to 3 could be assigned 140, 24, and 82 discontinuities, respectively. The mean discontinuity length of the discontinuity sets L_1, L_2, and L_3 are 4.51, 5.57, and $2.85\,\mathrm{m}$, respectively. The fracture densities d_1, d_2, and d_3 were derived as 2.23, 0.38, and $1.31\,\mathrm{m}^{-1}$, respectively. Although the fracture density of set 2 is very low compared to the other sets, the mean discontinuity length is relatively high and reaches $5.57\,\mathrm{m}$. The angles between the strike directions of sets 1 and 2, 1 and 3, and 2 and 3 are 115°, 87°, and 28°. The identified fracture properties of the sets result in an average number of discontinuity intersections per discontinuity of 3.71 for the exposed carbonate layer in Hagen Hohenlimburg.

3.2 Laboratory Characterizations

Samples could be obtained from all outcrops of dolomitic carbonates and limestone rocks, although it was challenging to obtain samples from the Hönnetal due to the lack of revealed outcrops. Most of the exposed Hönnetal limestone rocks were pure and showed a very low grade of dolomitization. Nevertheless, some dolomitic carbonates have been sampled. Dolomitic carbonates samples from Hagen Hohenlimburg occurred as highly fractured rocks with karst and highly porous formations ranging from a few millimeters to several centimeters. In total, from the collected rock blocks of the Wuppertal, Hagen Hohenlimburg, and Hönnetal outcrops six, eight, and six samples could be prepared, respectively. Furthermore, it was possible to drill a sample directly from the existing rock face in Hagen Hohenlimburg, that is described separately below.

The mean bulk densities of the samples retrieved from the outcrops in Wuppertal, Hagen Hohenlimburg, and Hönnetal were 2704 $\pm$39, 2537 $\pm$128, and 2620 $\pm$46 $\mathrm{kg\,m^{-3}}$, respectively (Table 4). These mean values were determined independently of whether they were limestone rocks or dolomitic carbonates. In Wuppertal as well as in Hagen Hohenlimbug, one dolomitic carbonate sample was investigated in each case, which differs significantly from the other samples and was not included in the

calculation of the mean bulk densities. Taking into account the measurement uncertainty and standard deviation, all samples examined showed comparable densities. A similar trend was observed for the mean grain densities, as these values are also very close together. The mean grain densities of the samples from Wupptertal, Hagen Hohenlimburg and Hönnetal amounted to 2801 $\pm$51, 2777 $\pm$41, and 2848 $\pm 32\,\mathrm{kg\,m^{-3}}$, respectively.

Laboratory measurements to determine the total and connected porosities indicated that the dolomitic carbonates investigated were significantly more porous than the limestones. This trend was evident at all quarries. The volumetric proportion of pores in the dolomitic carbonates was on average twice as high as in the limestones among almost all samples. Our uncertainty analysis showed that no significant volume of isolated pores and pre-existing cracks could be determined in the investigated samples. Taking into account the measurement uncertainties, the total and connected porosities overlapped (Fig. 8a).

Ultrasound P- and S-wave velocities of the dry samples ranged between 3000 and $6500\,\mathrm{m\,s^{-1}}$ and 1300 and $3500\,\mathrm{m\,s^{-1}}$, respectively. Regardless of the outcrop, it was shown that the dry P-wave velocities of the limestones tended to be 1000 to $1500\,\mathrm{m\,s^{-1}}$ higher than those of the dolomitic carbonates. The Wuppertal samples have shown that the dolomitic carbonates and limestones cannot be distinguished according to the S-wave velocities. Both rock types had comparable S-wave velocities. In contrast, the samples of the remaining outcrops showed a clear difference in S-wave velocities between dolomitic carbonates and limestone. In Hagen Hohenlimburg and Hönnetal the S-wave velocities of the limestones were about 500 to $1000\,\mathrm{m\,s^{-1}}$ higher than those of the dolomitic carbonates. These differences were also apparent in the drained dynamic Youngs' moduli. The mean drained Young's moduli of the limestone and the dolomitic carbonates amounted to about 60 and 70 GPa, respectively. The mean drained Poisson's ratio, that is, the relative relationship between P- and S-wave velocities, is about 0.35 for both rock types, taking into account the measurement uncertainties and the sample variability. Upon Saturation, P-wave velocities of the samples collected in Wuppertal, Hagen Hohenlimburg, and Hönnetal increased averagely by up to 4, 11, and $14\,\%$. This increase was also apparent in the undrained Poisson's ratios. The undrained Young's moduli hardly differ from the drained ones. In this case, increases of 1 to 3 GPa were mainly recorded.

The results of the measurements of the thermal conductivities showed a scattering, with a slight tendency that the mean thermal conductivity of the limestones is at least as high as the one of the dolomitic carbonates. The dolomitic carbonate samples from Wuppertal were an exception, as these samples showed relatively high thermal conductivities that even exceeded those of the limestones. On average, the highest and lowest conductivities could be determined on the Wuppertal and the Hagen Hohenlimburg samples, respectively. Measured thermal conductivities of all samples varied between 1.10 and $3.40\,\mathrm{W\,(m\,K)^{-1}}$.

The permeabilities measured correlated as expected with the corresponding porosities, that is, permeability increase with increasing proportion of connected pore volume (Fig. 8b; Table 4). The measured permeabilities of the dolomitic carbonates from Hagen Hohemlimburg are the highest and averaged to about $4.27 \times 10^{-16}\,\mathrm{m^2}$. The Hagen Hohenlimburg limestones were on average about three orders of magnitude less permeable than the limestones. The differences in permeability between dolomitic carbonates and limestone samples amounted to approximately two orders of magnitude in Wuppertal, whereas dolomitic carbonates and limestones in Hönnetal showed similar permeabilities of the same order of magnitude, that is, permeabilities in the range of $10^{-18}\,\mathrm{m^2}$. Only one sample from Hönnetal was low permeable (permeability of about $4 \times 10^{-20}\,\mathrm{m^2}$), but here the associated connected porosity was also significantly smaller than that of the comparative samples.

In the Hagen Hohenlimburg quarry, a healed vein in the limestone could be sampled directly in the outcrop. Before drilling, the orientations of the rock wall f_1 and the healed vein f_2 within the rock wall were recorded. The sample was drilled perpendicular to f_1 and parallel to f_2. The dip direction and angle of f_1 was $326°$ and $70°$ with respect to dip direction, respectively. In comparison, the measured dip orientation and angle of f_2 was $243°$ and $72°$ with respect to dip direction, respectively. During preparation, the cored sample was cut into two sections: S1 and S2. The laboratory investigations were carried out on the longer sample S2. This sample had high porosities of about $10\,\%$. Based on our laboratory measurements, and given the uncertainties, no isolated pore space could be determined. The dry as well as the saturated ultrasound velocities could not be distinguished from the ones of the dolomitic carbonates and limestone samples. Due to the saturation of the pore space with distilled water, an increase in the P-wave velocity of $10\,\%$ could be determined. Also, the thermal conductivity did not differ from the ones of the other samples from Hagen Hohenlimburg. The determined Poisson's ratio was the largest in this study, whereas the Young's modulus was in the lower range of all measured values. The permeability of this sample was determined under different pressures and a strong pressure dependence was shown. The relatively high permeability decreased by about one and a half orders of magnitude due to the minor increase of the stress state. At the highest applied pressure, however, the permeability also increased again by half an order of magnitude. An additional X-ray microtomography scan of the sample showed that the fracture connects both sample end faces but the fracture aperture exhibit large variations, that is, from open to closed.

4 Discussion

The discontinuities of deep carbonates in the Rhine-Ruhr area were characterized and described using outcrop scanline surveys. Also the results of laboratory investigations of density, porosity, dynamic elastic moduli, thermal conductivity, and permeability of the collected representative rock samples of the Devonian Reef Complex were presented. In the following, we correlate the field and laboratory investigations and address the geothermal potential of these deep carbonates in the Rhine-Ruhr region. We focus our results of the DFN on discontinuity length, density, orientation, and aperture. Characterizing the DFN requires an access to the reservoir rock at reservoir related depth which is not present. However, we have reasonable concerns to expect comparable discontinuity orientations in our geological subsurface model as in our studied outcrops (Lorenz et al., 1991; Narr, 1991). For example, Narr (1991, 1996) presented how to derive DFN from drill core samples of reservoirs.

4.1 Estimating the Geological Subsurface Model of the Carbonate Reservoir

The geological setting in the Rhine-Ruhr metropolitan area is highly complex, with details still being debated (e.g., Brix et al., 1988). However, we can name large tectonic events, which have influenced local formations to a varying extent:

1. Crustal thinning, which enhanced the formation of a shelf sea during the Early Devonian (e.g., Dallmeyer et al., 2013).

2. An overall NW-movement reduced clastic sedimentation within the sea and enabled the formation of reef carbonates on the clastic shelf. Beside those clastic shelf carbonates, other reef deposits formed on volcanic mounds within

the hemipelagic realm and is the geothermal horizon of interest in this study (e.g., Franke et al., 2017; Salamon and Königshof, 2010).

3. The ongoing NW-movement, which changed the material deposits and thus finally created the Ruhr coal district during the Carboniferous (e.g., Meschede, 2018).

4. At least two different extension sequences during the Early Triassic and Early Cretaceous (Drozdzewski and Wrede, 1994).

5. A NE-SW-directed shortening during the Late Cretaceous (e.g., Brix et al., 1988).

6. Further extensional regime since the Eocene (Kley, 2013).

Due to the complexity of the geological formation, our underground model has been simplified with respect to the most important tectonic features such as folds and faults. The foundation of our model is an approx. $150\,\mathrm{m}$ thick carbonate layer, dipping northwards at a dip angle of about 30 to 40 ° (see Fig. 1b Jansen et al., 1986; Drozdzewski et al., 2007). We expect this layer to be at depths between 4000 to $6000\,\mathrm{m}$ (DEKORP Research Group, 1990). This layer forms the Devonian basement, which is overlaid by interbedded sequences of sand, clay, silt, and coal layers from the Carboniferous period. These sediments can be mapped to the surface (e.g., Brix et al., 1988). Many folds and thrusts are found within these extremely complex interbedded sequences (for more details see Brix et al., 1988; Drozdzewski and Wrede, 1994).

All studied outcrops are located in the large scaled fold formation Remscheid-Altena anticline. However, there is a disagreement between the three outcrop results which might be an effect of the formation of the regional Remscheid-Altena anticline, different stress states, or different time of origin (Table 3). Due to the anticline formation, the strike directions of the present fractures in this region exhibit a rotation from the northern limb (Wuppertal) towards the tip of the anticline (Hönnetal). Fractures striking NE−SW are highly related to folding mechanism and are parallel oriented to fold axes which have been studied within the Rhine-Ruhr area (Drozdzewski, 1985; Brix et al., 1988; DEKORP Research Group, 1990; Drozdzewski and Wrede, 1994). The dominant fracture strike directions NNW−SSE in Wuppertal agree with the structure of the regional Remscheid-Altena anticline (Fig. 1b) and the overall assumed mean horizontal stress direction according to the World Stress Map (Heidbach et al., 2016) and additional available stress data (Rummel and Weber, 1993). In western Germany, or to be more precise in North Rhine-Westphalia, the World Stress Map contains a wide variability of mean horizontal stress directions (Heidbach et al., 2016), that can be explained by shallow stress measurements, local anomalies which can be attributed to weak coal-seems, or regional NE−SW thrusts. The observed strong scattering of the fracture strike directions in the dolomitic carbonates exposed in Hagen Hohenlimburg is due to their formation by hydrothermal veins during the Hercynian Orogney (Gillhaus et al., 2003). Furthermore, Gillhaus et al. (2003) explain that the existing NNW−SSE striking fractures are of post-Hercynian Orogeny origin. The cause of the slightly different fault strike directions in Hönnetal cannot be clearly specified according to the current state of scientific knowledge. Most likely, the fracture formation can be explained by various local and temporal stress anomalies and different formation times.

Brudy et al. (1997) showed that no significant stress orientation changes have to be expected in the brittle crust with depth. Consequently, it is reasonable to assume that we can expect quite similar discontinuity directions in our target horizon of the deep Devonian limestone, that is, the potential geothermal reservoir. However, if the carbonate layers exposed in the investigated opencast mines are extrapolated in dip direction of bedding, the carbonate reservoir of interest is approximately located below the cities Essen, Bochum, and Dortmund at depth of 4000 to $6000\,\mathrm{m}$ (Fig. 2). This extrapolation of the carbonates in dip direction corresponds in this case approximately to the direction of the main horizontal stress (Heidbach et al., 2016; Rummel and Weber, 1993) with respect to the simplified geological setting (Fig. 1a). This assumption allows us to predict local DFN in the deep Devonian limestone (i.e., naturally fractured carbonate reservoir), whose exact depth and characteristics should be verified by additional geophysical prospecting techniques to further describe the geothermal potential of this reservoir (e.g., Hirschberg et al., 2015).

We carried out laboratory experiments under ambient and elevated pressure conditions to gain insights into the petrophysical properties of the potential reservoir. The derived porosities of the limestone samples are in agreement with literature values between 1 and $6\,\%$ (Fig. 8a; c.f. Gebrande, 1982). The porosity of carbonate rocks may increase by a broad variation of processes. Next to dissolution, cementation, and recrystallization the process of dolomitization is the most common one. Dolomitization describes the geochemical process of replacing Ca ions by Mg ions, forming dolomite from calcite: $2\mathrm{CaCO_3} + \mathrm{Mg^{2+}} \rightarrow \mathrm{CaMg(CO_3)_2} + \mathrm{Ca^{2+}}$. Lucia et al. (2007) pointed out that dolomitization may increase the carbonates porosity by $13\,\%$. This correlates fairly well with our results (cf. Fig. 8a). Consequently, porosity measurements are in accordance with the outcome of the field study: porosity decreases towards core reef formation, in agreement with Homuth et al. (2015b).

The P- and S-wave velocities as well as the matrix permeabilities and dynamic mechanical properties derived in the laboratory provide statistical information for further numerical simulations of the reservoir. The thermal conductivity results are appropriate for the analyzed rock formations (c.f. Čermák and Rybach, 1982; Clauser and Huenges, 2013; Jorand et al., 2015). The low connected porosities match with the determined permeabilities. Compacted limestone (Massenkalk), which is characterised by a low connected porosity, showed the lowest permeability, whereas the dolomitic carbonates showed an inverse relation (see Fig. 8b). Although the results of the determined matrix permeability seem to be comparable with similar geothermal reservoirs (e.g., Homuth et al., 2015a), we do not expect sufficient reservoir permeability in 4000 and $6000\,\mathrm{m}$ depth. Therefore, we have focused on potential DFN within the geothermal reservoir, whose influence on fluid flow in fractured reservoirs has already been discussed in detail (e.g., Guerriero et al., 2013).

4.2 Evaluating a Discrete Fracture Network in the Carbonate Reservoir: From Outcrop and Laboratory Measurements to Implications for Fluid Flow on Reservoir Scale

The uncertainties associated with the description of naturally fractured systems and DFN are strongly dependent on sampling effects such as truncation or censoring (Bonnet et al., 2001; Baecher and Christian, 2005). Basically, truncation effects explain the influence of underestimating small characteristics due to the resolution of the sampling method, that is, outcrop and/or survey size. Censoring effects occur when large characteristics are incompletely observed due to the outcrop size mentioned or when characteristics are selected due to subjective choice (Priest and Hudson, 1981; Lacazette, 1991). While the trunctuation

effects ca be reduced by a sophisticated set of data and resolution, the censoring effect can be reduced depending on the method applied, adapted technology, and the amount of data obtained (Santos et al., 2015). In the literature these uncertainties are typically described as aleatory and epistemic (Der Kiureghian and Ditlevsen, 2009). Various survey methods and their corrections with regard to the effects mentioned are described in more detail in Bonnet et al. (2001).

The approach we have chosen to use the scanline survey method described by Priest and Hudson (1981) is a widely accepted method for the characterization of fracture networks (e.g., La Pointe and Hudson, 1985; Lacazette, 1991; Narr, 1996). The advantages of the method are especially the acquisition time and the associated verification as well as the acquisition costs compared to other methods (e.g., LIDAR outcrop survey; Wilson et al., 2011). The uncertainties due to scanline surveys are generally known and have been critically questioned for decades (e.g., Terzaghi, 1965; Cruden, 1977; La Pointe and Hudson, 1985; Ganoulis, 2008). However, due to the long period of application, the method explained by Priest and Hudson (1981) has been adapted for a variety of geological and outcrop settings, which leads to various error corrections regarding the application case. This allows us to keep the limitations and sources of error as low as possible. We pursued the concerns about epistemic uncertainties and identified the main problems in defining the locations of representative areas to evaluate a discrete fracture network in the carbonate reservoir in the Rhine-Ruhr area.

4.2.1 Orientation of the Fracture Network

The architecture of each open pit mine studied is directly related to the directions of the dominant discontinuities, that is, NNW−SSE and NE−SW (Fig. 3). Both rock faces are approximately perpendicular to each other in each quarry. The high angle between the scanline tape and the recorded fracture sets allows us to neglect the blind spots, as discussed in Lacazette (1991). In order to map all the features of the outcrop, we decided to carry out surveys at different levels of the quarry. The main discontinuity orientations were documented as NNW−SSE, NW−SE, and NE−SW. These results fit with the general observations documented in the literature (e.g., Brix et al., 1988). In addition, we present fracture orientations versus filling materials, these are, calcite or debris. The orientation of the recorded veins allows us to conclude, that many of the discontinuities studied on the outcrop scale can be related to residual stress and stress release during unloading regimes (cf. Nickelsen and Hough, 1967; Roberts, 1974, Fig. 7). It was observed that the regional fracture sets were continuous and consistent in orientation over large areas of several thousand square meters (Kelley and Clinton, 1960; Stearns and Friedman, 1972; Hancock and Bevan, 1987). When comparing the recorded discontinuity orientations with the orientation of the maximum horizontal stress (Heidbach et al., 2016), we propose to focus on discontinuities that are oriented NNW−SSE for future geothermal applications, which are highly probable filled by calcite. Pre-existing discontinuities oriented parallel to the maximum horizontal stress could be observed openly, while discontinuities oriented perpendicular to this stress tend to be closed (Lorenz et al., 1991). It can therefore be assumed that higher fracture permeability can be expected in the NNW−SSE direction, which could be of interest for the application of hydraulic stimulation techniques. In addition to the relative orientation of the fractures to the direction of the main principal stress, the filling is also decisive for whether the fractures are potentially open or closed in the subsurface (Laubach et al., 2004). Thus, there might be open fractures that are not necessarily aligned in the direction of

the principal stress and are still open. This is particularly true for fractures that are filled, for example, with cement (Laubach et al., 2004).

4.2.2 Filling and Surface Roughness of the Fracture Network

Information about fracture fillings and surface roughness can be used to estimate the reservoir behaviour under in-situ conditions, since fillings and roughness have a direct influence on the elastic, hydraulic and thermal properties of the reservoir. The presented results in this study can be used for a first impression of the petrophysical properties, like P- and S-wave velocity, of the host rock itself. The observation of filling materials, like calcite, indicate paleo fluid-flow paths which might be utilized by advanced drilling methods (e.g., hydraulic fracturing; Dahi Taleghani and Olson, 2013). Before utilizing, the material changes between host rock and vein material might be used to predict fracture orientations in depth by further geophysical driven studies (e.g., density changes, reflection coefficients). Further studies have to prove, if the material change between the encountered filling materials and the host rock is sufficient enough for seismic interpretation. More than half of all observations showed paleo filling materials like calcite beside calcite enriched slickensides on the fracture surface, approx. $58\,\%$ and $17\,\%$, respectively. This results into $25\,\%$ of fractures which might develop during other tectonic origins. The observed slight fracture rotation between paleo and recent or debris-filled discontinuities strongly suggests that the fill material may serve as an indication of their different tectonic origins. It is also remarkably that the average orientation of the recently filled cracks of the set 1 corresponds very well with the orientations of the main horizontal stress according to the World Stress Map (Heidbach et al., 2016) and additionally available stress data (Rummel and Weber, 1993). The unfilled fractures might be interpreted as open or closed in the subsurface. If the fractures appear to be open, fracture roughness is the next property which should be considered in deriving a proper geothermal model of the area.

It is very complex to determine fluid flow by both numerical and analytical methods along two irregular faces, that is, natural fracture surface. However, the impact on fluid flow along rough fracture surfaces was already shown and discussed (e.g., Brown, 1987). In the scope of this study, fracture roughness was ascertained qualitatively regarding the applied method. The results indicate predominating smooth fracture surfaces on the field scale ($> 10^{-1}\,\mathrm{m}$) and mainly slightly rough fracture surfaces on the mesoscopic scale ($\leqslant 10^{-1}\,\mathrm{m}$). In the literature roughness on field scale are typically described as waviness or straightness (ISRM, 1978). Verifying the determined roughness is only possible with difficulty. However, considering the numerous tectonic events and its repetitive reactivation of pre-existing fractures, smooth fractures tend to be reasonable.

4.2.3 Connectivity of the Fracture Network

The results of our scanline surveys revealed that discontinuities with short trace lengths occur predominantly on the field scale. This observation was made for all exposed outcrop faces in all three quarries. Almost $70\,\%$ of the recorded discontinuities classified as "both ends visible" tended to be between 1 and $2\,\mathrm{m}$ long. It is conceivable that the observed trace lengths increase with increasing outcrop length and height. The recorded end types suggest that $40\,\%$ of all discontinuities investigated exceeded the observed outcrop height. In other words: $40\,\%$ of all measured trace lengths might be underestimated by the method. This source of error was attempted to be minimized by the censored semi-trace length analysis according to Priest and Hudson

(1981). Contrary, 60 % of all joints counted showed a start and end tip (Table 2). However, a full 3D discontinuity analysis of the entire quarry will likely reflect better trace length results depending on the accuracy. At this point, economic considerations must be made regarding the required survey accuracy and associated costs. Regarding our joint analysis from Wuppertal, approx. 70 % of all observations are classified as short discontinuities (Table 3). In Hagen Hohenlimburg approx. 50 % of the observations are rather to be classified as short. In Hönnetal, approx. 47 % of all recorded joints had both ends determined. The comparison of the discontinuity track lengths with the true discontinuity distances gives a first idea of a connected fracture network. With reference to the mean trace lengths and mean true discontinuity distances recorded in Wuppertal, Hagen Hohenlimburg, and Hönnetal, we expect comparable probabilities for connected joint networks in each outcrop. However, our results of the 2D fracture connectivity analysis clearly show that the reservoir in Wuppertal has the highest average 2D fracture connectivity. Both the fracture density and the mean discontinuity length of each discontinuity set are significantly higher in Wuppertal than in the other outcrops. Accordingly, we can assume that this reservoir probably has considerable geothermal potential. For the Hönnetal reservoir a low number of discontinuity intersections per discontinuity was determined. One reason for this relatively low value is the location of the reservoir on the anticline axis and the associated tectonics. Although the recorded fractures in Hagen Hohenlimburg exhibit the greatest variety of strike directions, the estimated 2D fracture connectivity is the lowest at this location, which is due to the short discontinuity lengths and the associated low fracture densities. Nevertheless, based on the observations of many karst formations and altered host rocks by hydrothermal veins in Hagen Hohenlimburg, we conclude that there might be a higher permeability in the Hagen Hohenlimburg reservoir and in the surrounding areas than in the other studied areas. But, the distribution of this reservoir in the subsurface is still under debatte (e.g., Salamon and Königshof, 2010) and its conditions due to karstification still have to be proven.

The densities of the dolomitic carbonates and limestones determined in the laboratory did not show significant differences, which was to be expected, but the comparatively high porosity of the dolomitic carbonates indicated a moderate pore and crack volume. Consequently, on the one hand, it can be assumed that a higher density of potentially hydraulically stimulateable pores and cracks (or fracture network) is found in the dolomitic carbonate layers on the field scale. On the other hand, the comparable densities pose a warning regarding the unreflected interpretation of, for example, density measurements in naturally fractured carbonate reservoirs. Such measurements do not appear to be very useful for differentiating between low porous limestone and relatively high porous dolomitic carbonates. The influence of pore and crack volume in the dolomitic carbonate samples was also reflected in the measured ultrasonic velocities, as the dolomitic carbonate samples showed the lowest P-wave velocities. The S-wave velocities of dolomitic carbonates and limestones hardly differ, which is in good agreement with the given densities. A warning must also be given at this point, as the healed vein sample showed almost identical ultrasonic velocities compared to the other samples (Table 5). The saturation of the healed vein sample resulted in the smallest increase in P-wave velocity. Therefore, it is important to observe the temporal and spatial variation of the elastic wave velocities during a potential reservoir stimulation of the reservoir in order to get conclusions about its characteristics. In the next stage these findings can be of great importance for the interpretation of flow rates in the deep carbonate reservoir. Ahrens et al. (2018) demonstrated experimentally that there is an uniform correlation between P-wave velocity and the key parameter for transient flow processes, that is, hydraulic diffusivity, in the direction of fluid flow during inelastic deformation. Their observation

allows the conclusion that monitoring variations in P-wave velocities in field surveys can indicate changing fluid flow rates in, for example, evolving reservoirs. Consequently, these measurements bear the potential to give insights into deformation state, connectivity, and the hydraulic properties of pore and fracture networks in the reservoir.

The low impact of the fluid saturation on the dynamic moduli of the samples indicates that heterogeneous pore and/or crack networks prevail in the investigated samples. In the measuring or drilling direction of the samples only a small increase of the P-velocities and thus also of the undrained dynamic moduli occurs. This indicates that the connected pore and crack space tends to be locally distributed (c.f. upper Hashin-Shtrikman bound for a simplified two phase carbonate material; Hashin and Shtrikman, 1963), since ultrasonic velocities only characterize the momentary elastic behavior along a wave path, which was chosen by the waves due to its above-average rigidity. On the scale of wavelength, the samples are thus probably heterogeneous. Moreover, a velocity anisotropy should also prevail, which is particularly relevant for seismic surveys. However, a possibly existing heterogeneous and local distribution of the pore and crack volume has the advantage that it is more likely to encounter large pores and long and/or wide open cracks than would be possible with a homogeneous porosity distribution. It can be assumed that the heterogeneity possibly favours the fluid flow.

The sampled healded vein from Hagen Hohenlimburg exhibited a major pressure dependence of permeability in the range of the applied pressures, that suggests a rather low permeability ($< 10^{-18}$) of the target horizon in the expected depth. By means of hydraulic stimulation, however, the fractures prevailing there and their networks could possibly be reactivated, thus increasing the permeability. Eventhough this prediction clearly depends on the orientation of the fracture network in the stress field and the fluid pressure. However, for geothermal projects it is indispensable to carry out a seismic risk before planning to manipulate the local stress conditions, that is, the reactivation of fractures.

5 Conclusion

We investigated the geothermal potential of a carbonate reservoir in the Rhine-Ruhr area, Germany, by combining outcrop scanline surveys of pre-existing discontinuities and laboratory measurements of petrophysical properties on sample scale. The target horizon of interest is an approximately $150\,\mathrm{m}$ thick and widely distributed compacted limestone layer (Massenkalk) from Late Devonian in 4000 to $6000\,\mathrm{m}$ depth, dipping northwards at a dip angle of about 30 to 40 °. If we extrapolate the course of the exposed Devonian limestone layers, which were investigated at three outcrop analogues, in the direction of the maximum horizontal stress, the carbonate reservoir probably extends below Essen, Bochum, and Dortmund. Our petrophysical laboratory measurements on representative outcrop samples show that there is insufficient matrix porosity, permeability, and thermal conductivity in the reservoir rocks. This indicates that the characterisation of discrete fracture networks could be the key to the successful implementation of deep geothermal projects in the Rhine-Ruhr metropolitan region.

At the examined outcrops located within the Devonian Reef Complex, our scanline surveys revealed three main discontinuity orientations within the compacted limestones (NNW−SSW, NW−SE, and NE−SW) with dipping angles between 80 and $90°$. These discontinuity sets were in very good agreement with previously documented ones, that are the predominant orientations in the Rhine-Ruhr area with respect to the World Stress Map. With a simplified assumption that the stress state does not change

significantly with depth, it can be assumed that at least one of these fracture sets can be expected in the target horizon, that is, a naturally fractured carbonate reservoir. We propose to focus on discontinuities that are approximately NNW−SSE oriented for upcoming geothermal applications, considering that this direction is approximately parallel to the maximum horizontal stress. Hence, possibly opened fractures with higher permeability could be expected here.

The results of our comprehensive scanline surveys also provided information about the possible filling and surface roughness, which are of significant importance for estimating the fluid flow in the reservoir. More than half of all observations showed paleo-filling materials such as calcite beside calcite enriched slickensides on the fracture surface. The recently debris-filled fractures are striking NNW−SSE and in the maximum horizontal stress direction. Thus, these fractures could possibly be reactivated and enhance fluid flow in the carbonate reservoir. The measured fracture sets showed mainly smooth and slightly rough fracture surfaces on the field scale and the mesoscopic scale, respectively. Considering the numerous tectonic events in the Rhine-Ruhr region and the resulting repeated reactivation of pre-existing fractures, slightly smooth fracture surfaces are more likely to occur in the reservoir. Discontinuities sets with short trace lengths occurred predominantly in all three outcrops. Almost $70\,\%$ of the recorded discontinuities classified as "both ends visible" tended to be between 1 and $2\,\mathrm{m}$ long. We compared the mean trace lengths with the mean true discontinuity spacing in order to get an idea of a coherent fracture network in the reservoir. Our 2D fracture connectivity analysis has shown that the reservoir of interest below Essen and located on the northern limb of the anticline most likely bears a well connected fracture network, because the reference reservoir in Wuppertal shows a high fracture connectivity. Besides, taking all measurements into account, we expect similar probabilities for interconnecting fracture networks in the deep reservoir. From this it follows that the recorded field surveys (Wuppertal, Hagen Hohenlimburg, and Hönnetal) can be assigned representatively for the reservoir of interest below the cities Essen, Bochum, and Dortmund. However, based on the observations of many karst formations and altered host rocks by hydrothermal veins in Hagen Hohenlimburg, we conclude that the permeability is greater in the regions of the Devonian reef facies than in the other areas investigated. This assumption was also confirmed by our laboratory measurements, whose results suggest the presence of heterogeneities that may favours fluid flow.

Our presented results may provide the basis for improved subsurface characterization with respect to the structure and characteristics of the naturally fractured Devonian limestone reservoir in the Rhine-Ruhr area. More sophisticated geophysical prospecting techniques and a combination of pressure and temperature dependent laboratory measurements have to elaborated to further verify the reservoir depth, orientation as well as its fracture density and connectivity. Further studies have to prove, if the fractures prevailing could possibly be reactivated and/or connected to fracture network, thus enhancing fluid flow in the carbonate reservoir. In addition to further discontinuity properties, the local stress field should be further verified in follow-up studies. The understanding of the structural characteristics of the fracture network and their impact on the elastic, thermal, and hydraulic properties of the reservoir that in turn defines the geothermal potential will benefit from, for instance, seismic surveys and in-situ measurements in a pilot borehole.

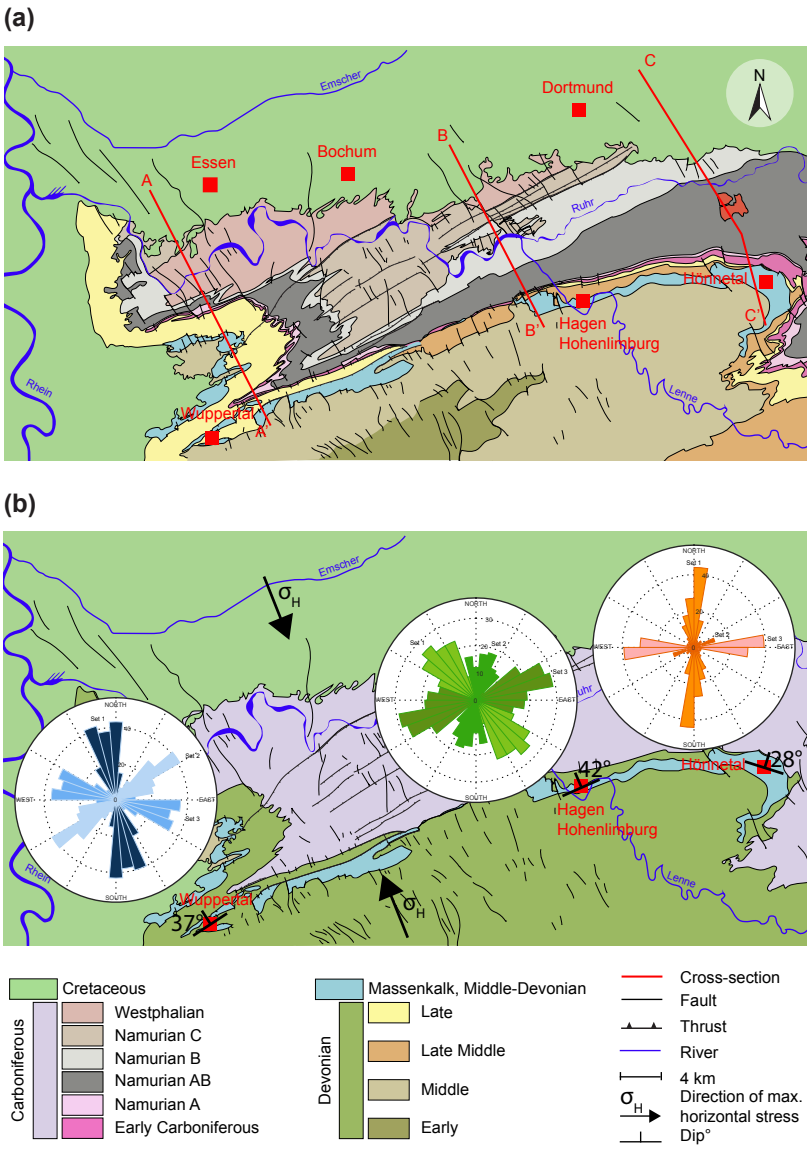

Figure 1. (a) Simplified geological map of the Rhine-Ruhr metropolitan area, Germany (modified after Jansen et al., 1986; Drozdzewski et al., 2007). Here, three stone pits have been chosen for field surveys: Osterholz (Wuppertal), Oege (Hagen), and Asbeck (Hönnetal), which are part of the Devonian Reef Complex (Massenkalk). The red lines indicate the three geological cross-sections as shown in Figure 2. In (b), the geological map from (a) was further simplified and in addition the rose diagrams of the discontinuity sets as measured by scanline investigations at the quarries in Wuppertal (blue), Hagen Hohenlimburg (green), and Hönnetal (orange) are added (for more details see Figs. 4 to 6). The arrows indicate the direction of maximum horizontal stress σ_{H} according to the World Stress Map (Heidbach et al., 2016). The specific directions and angles of incidence of the investigated, exposed Limestone layers are also shown in (b).

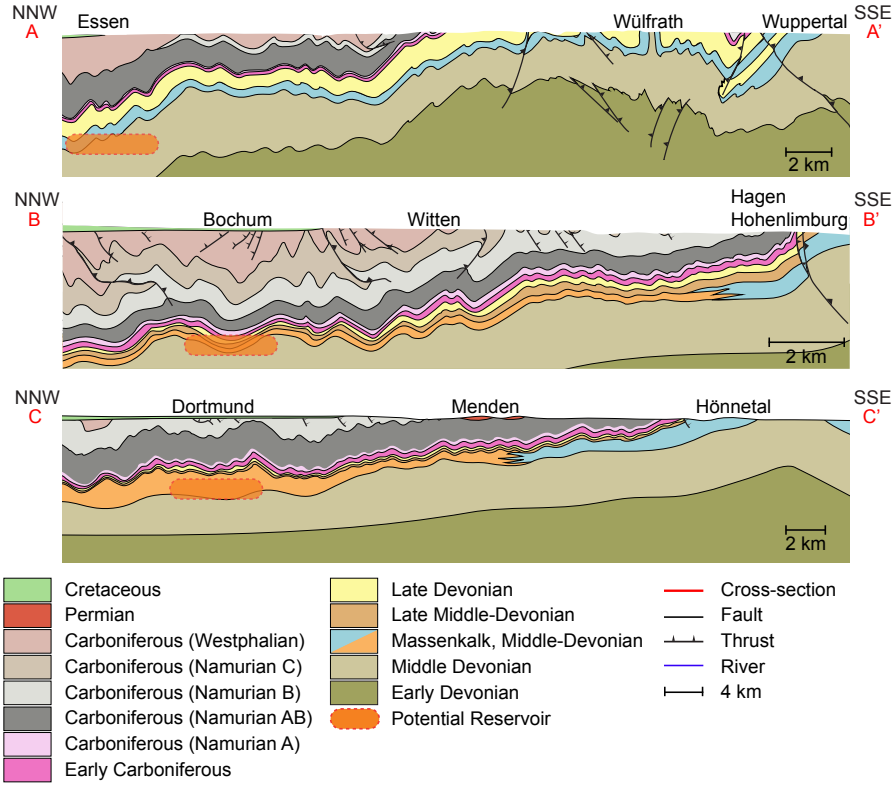

Figure 2. Simplified cross-sections of the Remscheid-Altena anticline (modified after Jansen et al., 1986; Drozdzewski et al., 2007). The exact position and orientation of the three cross-sections is illustrated in Figure 1a.

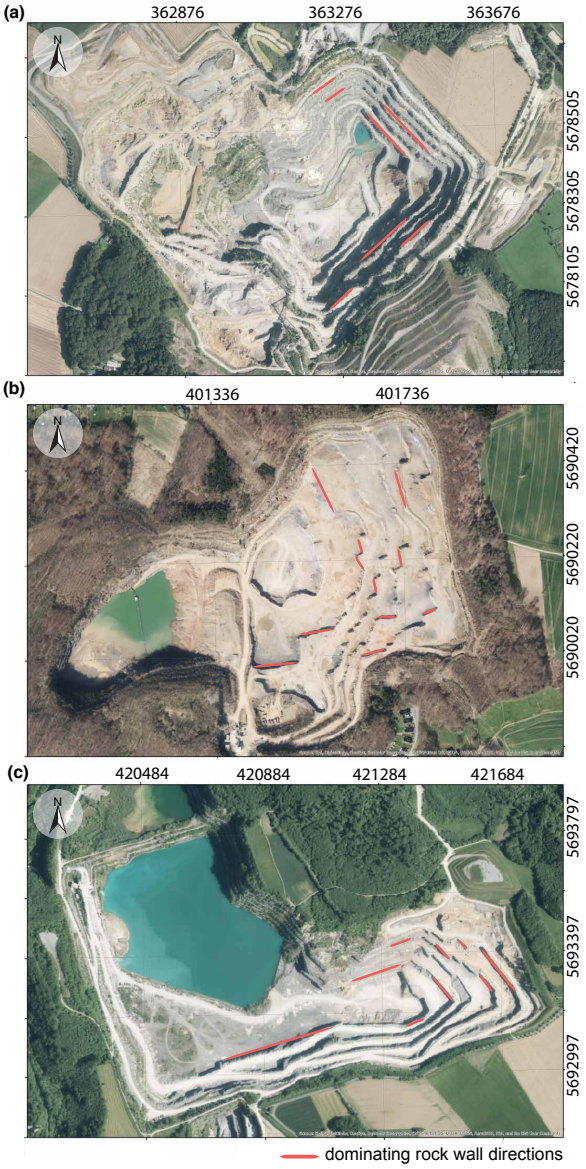

Figure 3. Map view of all three study areas in which scanline surveys were carried out: (a) The Osterholz stone pit, which was operated by Kalkwerke H. Oetelshofen GmbH & Co. KG in Wuppertal. (b) The Oege stone pit operated by Hohenlimburger Kalkwerke GmbH in Hagen Hohenlimburg. (c) The Asbeck rock mine managed by Lhoist Deutschland, Rheinkalk GmbH in Hönnetal. Red lines indicate the predominant rock walls, that is, the direction of mining. In each of the three outcrops there were two dominant mining directions, which were approximately perpendicular to each other. This figure was created using ArcGIS® software by Esri (Basemap, World Imagery: http://www.arcgis.com/home/item.html?id=10df2279f9684e4a9f6a7f08febac2a9). ArcGIS© and ArcMap™ are the intellectual property of Esri and are used herein under license. Copyright © Esri. All rights reserved. For more information about Esri™ software, please visit www.esri.com.

Table 1. Overview of the documented discontinuity properties and their classification as defined for scanline surveys according to Markovaara-Koivisto and Laine (2012). The roughness of the discontinuities was classified on field scale ($> 10^{-1}$ m) and on mesoscopic scale ($\leqslant 10^{-1}$ m).

property	class				
	1	2	3	4	5
discontinuity type	open	closed	filled	slickensides	dyke
ending type	through going	both ends visible	one end visible	neither ends visible	–
filling	calcite	debris	quartz	clay	–
roughness on field scale	smooth	slightly rough	rough	–	–
roughness on mesoscopic scale	smooth	slightly rough	rough	–	–

Table 2. Overview of the recorded properties and their classification of the measured discontinuities in the three studied outcrops in Wuppertal, Hagen Hohenlimburg, and Hönnetal. See text and Table 1 for a detailed description of the classes.

outcrop	property	class					total
		1	2	3	4	5	
Wuppertal	discontinuity type	129	110	113	109	–	461
	ending type	4	356	93	8	–	461
	filling	116	74	–	80	–	270
	roughness at field scale	354	81	26	–	–	461
	roughness at mesoscopic scale	159	250	52	–	–	461
Hagen Hohenlimburg	discontinuity type	86	52	156	67	–	361
	ending type	20	300	37	4	–	361
	filling	160	67	–	31	–	258
	roughness at field scale	194	116	51	–	–	361
	roughness at mesoscopic scale	77	184	100	–	–	361
Hönnetal	discontinuity type	51	51	121	23	–	246
	ending type	29	116	96	5	–	246
	filling	137	45	–	6	–	188
	roughness at field scale	216	26	4	–	–	246
	roughness at mesoscopic scale	55	155	36	–	–	246
all outcrops	discontinuity type	266	213	390	199	–	1068
	ending type	53	772	226	17	–	1068
	filling	413	186	–	117	–	716
	roughness at field scale	764	223	81	–	–	1068
	roughness at mesoscopic scale	291	589	188	–	–	1068

Table 3. Overview of the settings and the results of the scanline surveys performed on rock walls in the outcrops Wuppertal (WOH), Hagen Hohenlimburg (HKW), and Hönnetal (HLO). The abbreviations MKY, MKB, and MKR correspond to the coloured rock types Massenkalk yellow (dolomite), Massenkalk black (limestone), and Massenkalk red (dolomite), respectively. Three main families or sets of discontinuity orientations were found to be predominant in all outcrops.

scanline survey	l_{scan}	n	$\bar{l}_{\mathrm{dis}}$	$\bar{h}_{\mathrm{dis}}$	$\bar{d}_{\mathrm{dis}}$	discontinuity orientation (dipdir/dip)		
	(m)	(-)	(m)	(m)	(m)	set 1	set 2	set 3
WOH-2-MKB-1	9.70	74	1.63	< 0.01	0.13	329/89	237/84	–
WOH-3-MKB-1	12.22	84	1.64	< 0.01	0.15	259/87	190/87	–
WOH-4-MKB-1	14.10	58	2.31	< 0.01	0.25	265/85	150/86	–
WOH-4-MKB-2	8.10	39	0.92	< 0.01	0.20	146/70	193/81	270/88
WOH-4-MKY-1	5.92	81	3.14	< 0.01	0.08	247/89	198/88	–
WOH-4-MKY-2	3.94	44	0.56	< 0.01	0.09	261/84	203/65	–
WOH-5-MKB-1	10.10	59	0.87	< 0.01	0.20	259/87	135/77	–
WOH-5-MKB-2	2.52	22	0.85	< 0.01	0.11	268/83	313/69	038/69
HKW-2-MKB-1	17.40	41	2.75	0.02	0.43	240/87	–	–
HKW-2-MKB-2	9.90	42	3.58	0.03	0.24	333/71	–	–
HKW-3-MKB-1	5.80	36	0.77	< 0.01	0.19	290/89	348/70	–
HKW-3-MKB-2	4.75	30	0.54	< 0.01	0.22	194/71	–	–
HKW-1-MKY-1	17.30	97	0.58	< 0.01	0.21	207/83	–	–
HKW-4-MKB-1	6.80	40	0.54	< 0.01	0.20	277/87	175/81	–
HKW-5-MKB-1	7.43	14	0.76	< 0.01	0.28	212/82	–	–
HKW-5-MKY-4	6.80	46	0.23	< 0.01	0.36	351/86	284/82	212/82
HLO-4-MKB-1	13.66	50	3.31	< 0.01	0.30	351/75	–	–
HLO-4-MKB-2	10.00	49	2.32	< 0.01	0.21	176/77	–	–
HLO-6-MKB-1	17.70	34	6.77	0.06	0.53	254/87	018/86	–
HLO-6-MKB-2	10.80	30	3.55	0.01	0.40	253/81	134/74	195/86
HLO-6-MKB-3	10.60	84	4.67	0.02	0.14	271/89	–	–

l_{scan}: scanline length; n: number of discontinuities; $\bar{l}_{\mathrm{dis}}$: mean trace length; $\bar{h}_{\mathrm{dis}}$: mean discontinuity aperture; $\bar{d}_{\mathrm{dis}}$: mean discontinuity spacing. The resolution of the length measurements amounts to $0.01\,\mathrm{m}$.

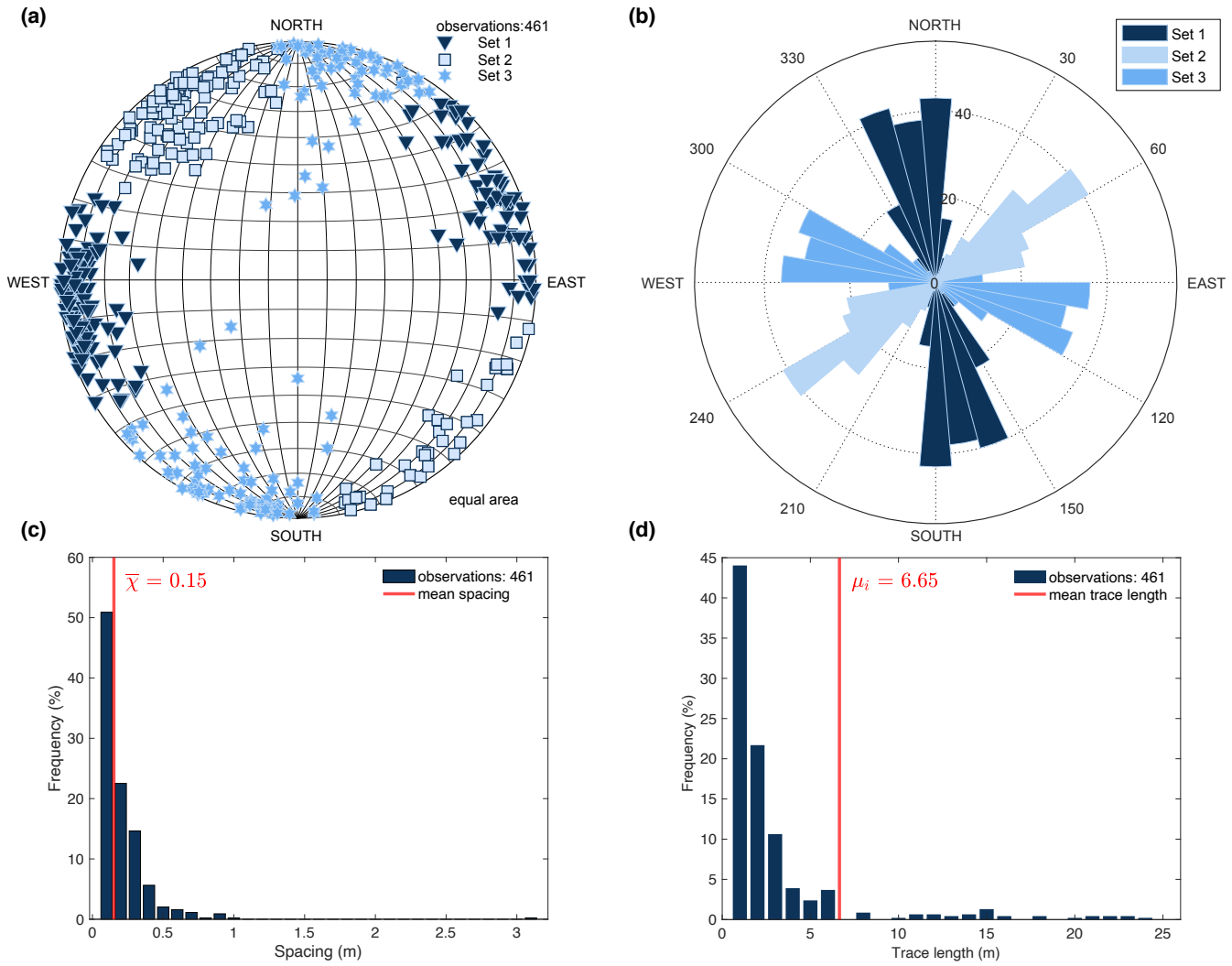

Figure 4. Results of all scanline investigations at the quarry in Wuppertal: (a) stereogram, and (b) rose diagram of measured discontinuity sets, (c) discontinuity spacing diagram, (d) discontinuity trace length diagram.

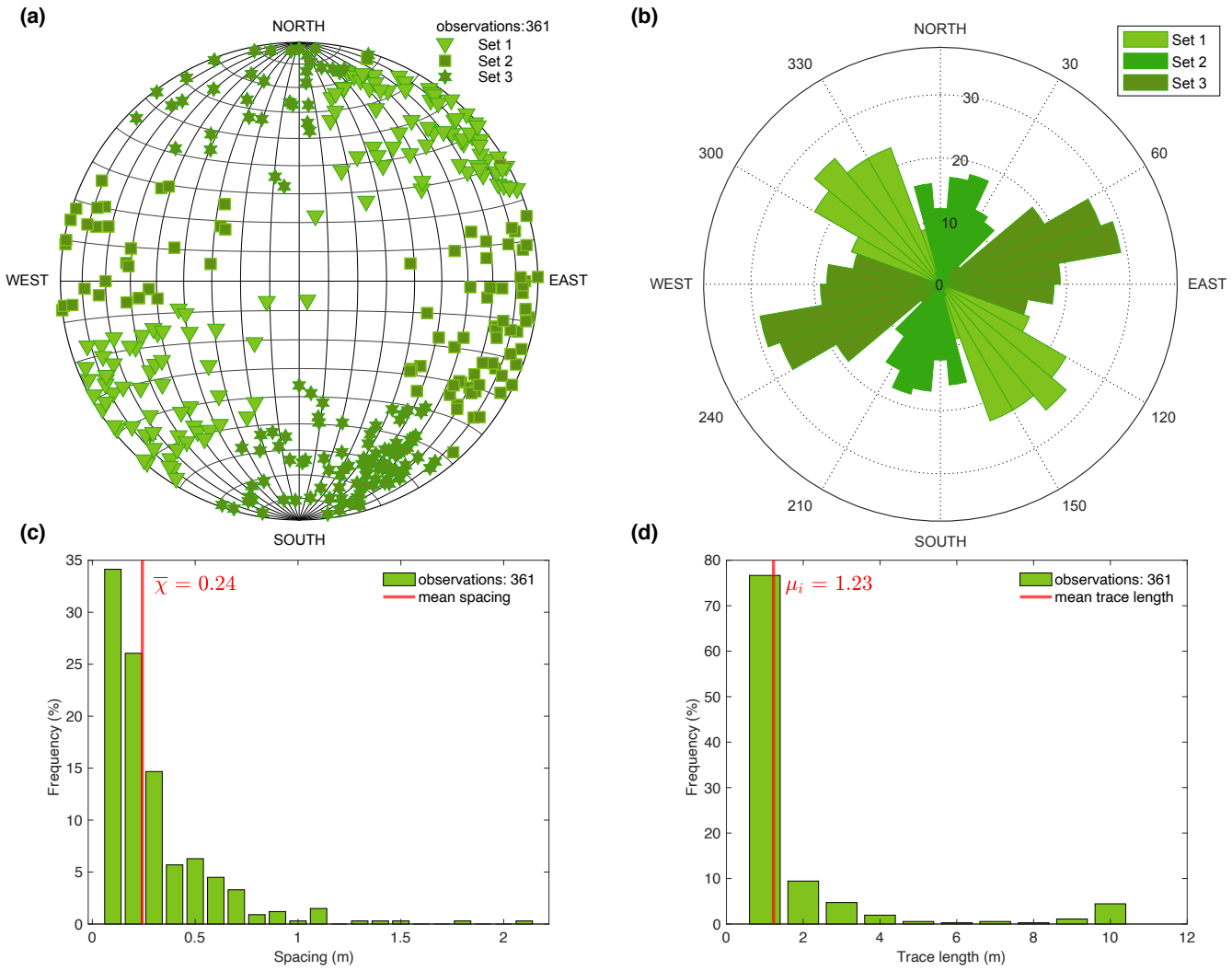

Figure 5. Results of all scanline investigations at the quarry in Hagen Hohenlimburg: (a) stereogram, and (b) rose diagram of measured discontinuity sets, (c) discontinuity spacing diagram, (d) discontinuity trace length diagram.

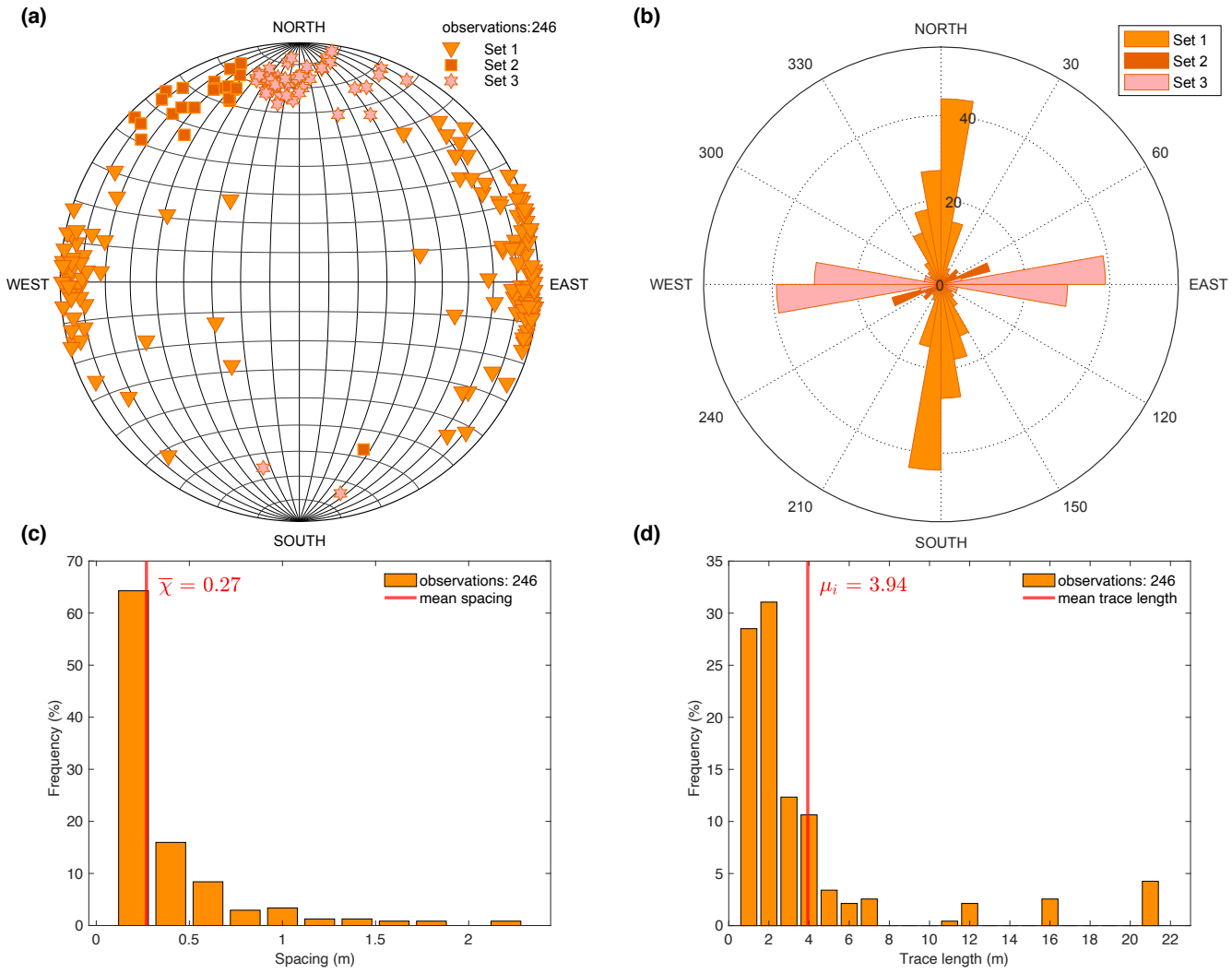

Figure 6. Results of all scanline investigations at the quarry in Hönnetal: (a) stereogram, and (b) rose diagram of measured discontinuity sets, (c) discontinuity spacing diagram, (d) discontinuity trace length diagram.

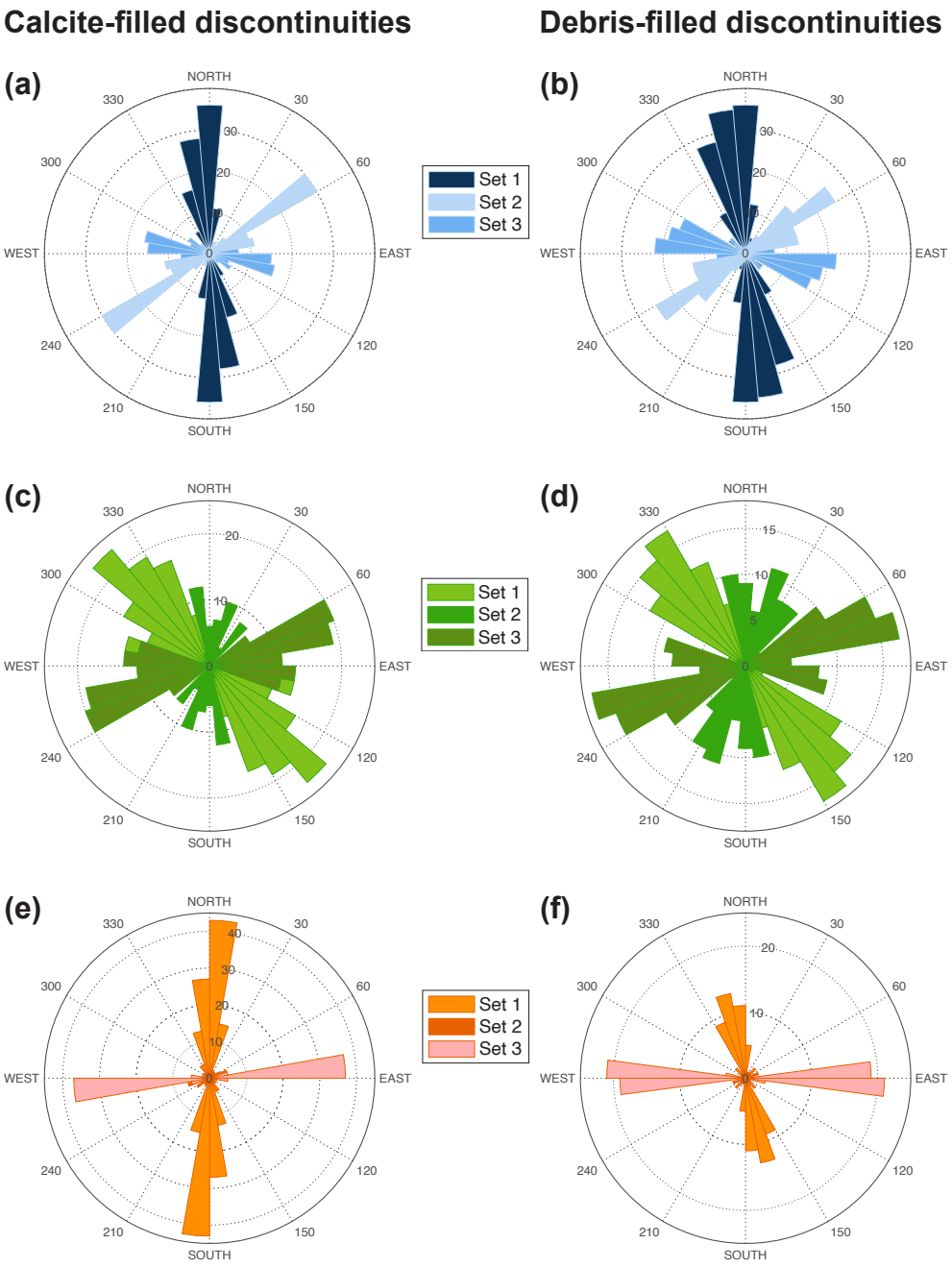

Figure 7. Rose diagrams of all measured discontinuity sets at the quarries (a, b) Wuppertal, (c, d) Hagen Hohenlimburg, and (e, f) Hönnetal as a function of their fracture filling, that is, whether the fractures are filled with (a, c, e) calcite or (b, d, f) debris.

Table 4. Matrix properties, permeabilities, and thermal conductivities as determined by laboratory measurements on limestone and dolomite samples from Wuppertal (WOH), Hagen Hohemlimburg (HKW), and Hönnetal (HLO). The abbreviations MKY, MKB, and MKR indicate the colored rock types Massenkalk yellow (dolomite), Massenkalk black (limestone), and Massenkalk red (dolomite), respectively.

sample	l (mm)	ρ_{geo} ($\mathrm{kg\,m^{-3}}$)	ρ_{grain} ($\mathrm{kg\,m^{-3}}$)	ϕ_{tot} (%)	ϕ_{con} (%)	k ($\mathrm{m^2}$)	κ_{dry} ($\mathrm{W\,(m\,K)^{-1}}$)
WOH-4-MKY-3 A	62.28	2695 ± 7	2801 ± 1	4.1 ± 1.8	4.1 ± 0.7	$(2.90 \pm 0.10) \times 10^{-18}$	2.64 ± 0.08
WOH-4-MKY-3 B	83.99	2787 ± 7	2830 ± 1	1.5 ± 1.8	6.0 ± 1.0	$(1.80 \pm 0.07) \times 10^{-18}$	3.02 ± 0.09
WOH-4-MKY-3 C	55.08	1755 ± 5	–	–	2.5 ± 0.4	$(5.30 \pm 0.20) \times 10^{-17}$	3.33 ± 0.09
WOH-4-MKB-1 A	83.53	2706 ± 7	2712 ± 1	0.2 ± 1.8	1.7 ± 0.3	$(1.90 \pm 0.07) \times 10^{-20}$	2.62 ± 0.08
WOH-4-MKB-1 B	82.05	2698 ± 7	2801 ± 1	3.7 ± 1.8	1.7 ± 0.3	$(1.60 \pm 0.06) \times 10^{-19}$	2.63 ± 0.08
WOH-4-MKB-1 C	82.91	2704 ± 7	–	–	1.7 ± 0.3	$(1.90 \pm 0.07) \times 10^{-20}$	2.63 ± 0.08
HKW-4-MKR-1 A	29.18	2558 ± 8	2771 ± 1	7.7 ± 1.8	7.1 ± 1.2	$(2.20 \pm 0.09) \times 10^{-16}$	2.18 ± 0.06
HKW-4-MKR-1 B	41.59	2420 ± 7	2779 ± 1	12.9 ± 1.8	14.0 ± 2.3	$(1.00 \pm 0.04) \times 10^{-15}$	3.36 ± 0.10
HKW-4-MKR-1 C	39.31	2018 ± 6	–	–	14.7 ± 2.4	$(7.60 \pm 0.32) \times 10^{-16}$	2.38 ± 0.07
HKW-4-MKY-2 A	39.39	2389 ± 7	2770 ± 1	13.8 ± 1.8	10.7 ± 1.8	$(2.40 \pm 0.10) \times 10^{-17}$	2.19 ± 0.06
HKW-4-MKY-2 B	34.13	2420 ± 7	2768 ± 1	12.9 ± 1.8	10.3 ± 1.7	$(1.30 \pm 0.05) \times 10^{-16}$	2.13 ± 0.06
HKW-5-MKB-1 A	83.89	2682 ± 7	2777 ± 1	3.4 ± 1.8	1.8 ± 0.3	$(4.90 \pm 0.20) \times 10^{-20}$	2.62 ± 0.08
HKW-5-MKB-1 B	74.30	2660 ± 7	2772 ± 1	4.0 ± 1.8	2.7 ± 0.4	$(1.40 \pm 0.06) \times 10^{-18}$	2.56 ± 0.08
HKW-5-MKB-1 C	76.92	2707 ± 7	–	–	1.3 ± 0.2	$(2.40 \pm 0.10) \times 10^{-19}$	2.52 ± 0.08
HKW-2-MKB-2-S2	92.25	2516 ± 7	2777 ± 0.2	9.4 ± 1.8	9.8 ± 1.6	see Table 6	3.00 ± 0.09
HLO-6-MKY-1 A	80.43	2541 ± 7	2820 ± 1	9.9 ± 1.8	4.6 ± 0.8	$(6.60 \pm 0.26) \times 10^{-18}$	2.33 ± 0.07
HLO-6-MKY-1 B	57.01	2621 ± 7	2875 ± 1	8.8 ± 1.7	5.6 ± 0.9	$(3.30 \pm 0.13) \times 10^{-18}$	2.45 ± 0.07
HLO-6-MKY-1 C	58.05	2611 ± 5	–	–	5.6 ± 0.9	$(4.20 \pm 0.17) \times 10^{-18}$	2.15 ± 0.06
HLO-6-MKB-3 A	81.32	2682 ± 7	2820 ± 1	4.9 ± 1.8	2.4 ± 0.4	$(3.80 \pm 0.15) \times 10^{-20}$	2.67 ± 0.08
HLO-6-MKB-3 B	47.16	2643 ± 7	2875 ± 1	8.1 ± 1.7	4.3 ± 0.7	$(2.60 \pm 0.10) \times 10^{-18}$	2.71 ± 0.08
HLO-6-MKB-3 C	41.53	2619 ± 7	–	–	3.7 ± 0.6	$(2.20 \pm 0.09) \times 10^{-18}$	2.60 ± 0.08

l: sample length; ρ_{geo}: bulk density; ρ_{grain}: grain density; ϕ_{tot}: total porosity; ϕ_{con}: connected porosity; k: permeability; κ_{dry}: thermal conductivity. Quoted uncertainties reflect accuracy of the measurements.

Table 5. Ultrasound velocities and dynamic elastic moduli derived by laboratory measurements for limestone and dolomite samples from Wuppertal (WOH), Hagen Hohemlimburg (HKW), and Hönnetal (HLO). The abbreviations MKY, MKB, and MKR indicate the colored rock types Massenkalk yellow (dolomite), Massenkalk black (limestone), and Massenkalk red (dolomite), respectively.

sample	$v_{\mathrm{P,dry}}$ (ms^{-1})	$v_{\mathrm{S,dry}}$ (ms^{-1})	$v_{\mathrm{P,wet}}$ (ms^{-1})	$\tilde{\nu}_{\mathrm{d}}$ ($-$)	$\tilde{\nu}_{\mathrm{ud}}$ ($-$)	$\tilde{E}_{\mathrm{d}}$ (GPa)	$\tilde{E}_{\mathrm{ud}}$ (GPa)
WOH-4-MKY-3 A	5660 ± 20	2990 ± 200	6420 ± 30	0.31 ± 0.13	0.36 ± 0.09	63 ± 8	65 ± 6
WOH-4-MKY-3 B	5590 ± 20	2850 ± 140	5800 ± 20	0.30 ± 0.10	0.34 ± 0.07	62 ± 6	63 ± 5
WOH-4-MKY-3 C	5790 ± 40	2929 ± 340	6086 ± 40	0.33 ± 0.13	0.35 ± 0.10	61 ± 8	62 ± 7
WOH-4-MKB-1 A	6430 ± 20	3120 ± 170	6470 ± 20	0.34 ± 0.08	0.35 ± 0.08	71 ± 6	71 ± 6
WOH-4-MKB-1 B	6310 ± 20	3030 ± 160	6520 ± 20	0.35 ± 0.08	0.36 ± 0.07	67 ± 5	67 ± 5
WOH-4-MKB-1 C	6380 ± 20	2800 ± 140	6480 ± 20	0.38 ± 0.06	0.38 ± 0.05	59 ± 3	59 ± 3
HKW-4-MKR-1 A	4050 ± 30	1740 ± 150	5580 ± 50	0.39 ± 0.09	0.45 ± 0.05	21 ± 2	22 ± 1
HKW-4-MKR-1 B	2970 ± 10	1350 ± 60	4330 ± 20	0.37 ± 0.06	0.44 ± 0.03	12 ± 1	13 ± 1
HKW-4-MKR-1 C	4050 ± 20	2230 ± 180	6050 ± 40	0.28 ± 0.18	0.42 ± 0.07	26 ± 5	29 ± 2
HKW-4-MKY-2 A	4530 ± 20	2460 ± 220	5430 ± 30	0.29 ± 0.19	0.37 ± 0.10	37 ± 7	40 ± 5
HKW-4-MKY-2 B	4810 ± 30	2570 ± 280	5210 ± 40	0.30 ± 0.21	0.34 ± 0.17	41 ± 9	43 ± 7
HKW-5-MKB-1 A	6450 ± 20	3320 ± 190	6560 ± 20	0.32 ± 0.10	0.33 ± 0.09	78 ± 8	78 ± 8
HKW-5-MKB-1 B	6190 ± 20	3380 ± 220	6350 ± 20	0.29 ± 0.14	0.30 ± 0.12	78 ± 11	79 ± 10
HKW-5-MKB-1 C	6410 ± 20	2770 ± 140	7120 ± 30	0.39 ± 0.06	0.41 ± 0.05	57 ± 3	58 ± 3
HKW-2-MKB-2-S2	5125 ± 13	2150 ± 71	5600 ± 15	0.39 ± 0.03	0.42 ± 0.03	32 ± 1	33 ± 1
HLO-6-MKY-1 A	5027 ± 14	2540 ± 115	6440 ± 20	0.33 ± 0.07	0.41 ± 0.04	43 ± 3	46 ± 2
HLO-6-MKY-1 B	5183 ± 20	2530 ± 160	6200 ± 30	0.34 ± 0.10	0.40 ± 0.06	45 ± 5	47 ± 3
HLO-6-MKY-1 C	3628 ± 10	2419 ± 140	5930 ± 30	0.10 ± 0.27	0.40 ± 0.06	34 ± 9	43 ± 2
HLO-6-MKB-3 A	6255 ± 20	3120 ± 170	6450 ± 20	0.34 ± 0.09	0.35 ± 0.08	74 ± 6	74 ± 6
HLO-6-MKB-3 B	5822 ± 32	3210 ± 300	6200 ± 40	0.28 ± 0.21	0.31 ± 0.17	70 ± 15	72 ± 13
HLO-6-MKB-3 C	5849 ± 40	3500 ± 400	6290 ± 40	0.22 ± 0.35	0.28 ± 0.27	78 ± 28	82 ± 23

$v_{\mathrm{P,dry}}$, $v_{\mathrm{P,wet}}$: P-wave velocity of dry and wet samples; $v_{\mathrm{S,dry}}$: S-wave velocity of dry samples; $\tilde{\nu}_{\mathrm{d}}$: dynamic drained Poission's ratio; $\tilde{\nu}_{\mathrm{ud}}$: dynamic undrained Poission's ratio; $\tilde{E}_{\mathrm{d}}$: dynamic drained Young's modulus; $\tilde{E}_{\mathrm{ud}}$: dynamic undrained Young's modulus. Quoted uncertainties reflect accuracy of the measurements.

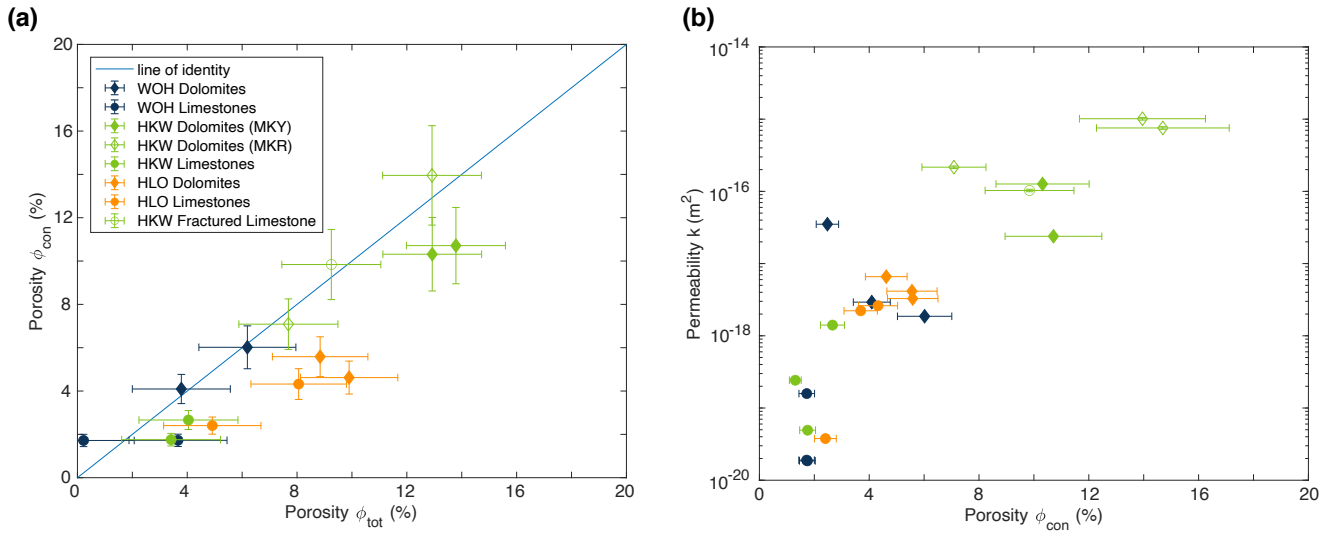

Figure 8. Correlation between (a) permeability and connected porosity and correlation between (b) connected and total porosity. Filling and coloring of markers indicate sample and outcrop, respectively. Measurement uncertainties are indicated by error bars. Where error bars do not exceed marker size, uncertainties appear to be small. The blue line in (b) indicates identity, that is, connected is equal to total porosity.

Table 6. Permeability of sample HKW-2-MKB-2-S2 as derived at different stress states. This limestone sample (MKB: Massenkalk black) was cored directly from a healed vein at an exposed limestone wall in the outcrop of Hagen Hohenlimburg (HKW).

sample	axial load (MPa)	confining pressure (MPa)	k (m^2)
HKW-2-MKB-2-S2	7	5	$(4.7 \pm 0.2) \times 10^{-16}$
	12	10	$(1.0 \pm 0.4) \times 10^{-18}$
	17	15	$(5.9 \pm 0.2) \times 10^{-18}$

k: permeability; Quoted uncertainties reflect accuracy of the measurements.

Acknowledgements. We thank all students and researchers involved in field and laboratory measurements, in particular Mathias Nehler. MB, BA, and EHS acknowledge generous funding by the Federal Ministry of Education and Research for the project 3D-RuhrMarie ("FHprofUnt2016"). KL thanks the "Ministerium für Innovation, Wissenschaft und Forschung des Landes Nordrhein-Westfalen" for funding of the project GREENER ("FH ZEIT für FORSCHUNG"). We especially thank the Geological Survey of North Rhine-Westphalia for providing maps and other information, as well as John Hooker and Sadegh Karimpouli for fruitful discussions and helpful comments on the earlier draft of the manuscript.

Financial support. This research has been funded by the 3D-RuhrMarie project ("FHprofUnt2016"), ComLabgo project ("FH ZEIT für FORSCHUNG"), and GREENER project ("FH ZEIT für FORSCHUNG").

Competing interests. The authors declare that they have no conflict of interest.

Data availability. The measured values and results recorded within the study are available on reasonable request from the corresponding author.

Author contributions. Four authors have contributed to this paper. MB was the lead author and carried out the field investigations, laboratory measurements, and analytical calculations. BA helped with the laboratory measurements on transport and elastic properties. KL was involved in the field investigations. EHS provided helpful background knowledge. MB and BA were involved in the data interpretation and writing of the manuscript.

References

AGFW: Arbeitsgemeinschaft für Wärme und Heizkraftwirtschaft: Technisches Handbuch Fernwärme, Technik und Normung, AGFW-Projektges. für Rationalisierung, Information und Standardisierung, 2009.

Agosta, F., Alessandroni, M., Antonellini, M., Tondi, E., and Giorgioni, M.: From fractures to flow: A field-based quantitative analysis of an outcropping carbonate reservoir, Tectonophysics, 490, 197–213, https://doi.org/10.1016/j.tecto.2010.05.005, 2010.

Ahrens, B., Duda, M., and Renner, J.: Relations between hydraulic properties and ultrasonic velocities during brittle failure of a low-porosity sandstone in laboratory experiments, Geophys. J. Int., 212, 627–645, https://doi.org/10.1093/gji/ggx419, 2018.

Araújo, K.: The emerging field of energy transitions: progress, challenges, and opportunities, Energy Res. Soc. Sci, 1, 112–121, https://doi.org/10.1016/j.erss.2014.03.002, 2014.

Attewell, P. B. and Farmer, I. W.: Principles of Engineering Geology, Springer Science & Business Media, London, 1976.

Baecher, G. B. and Christian, J. T.: Reliability and statistics in geotechnical engineering, John Wiley & Sons, Chichester, 2005.

Basse, M., Koch, L., and Lemke, U.: Torleyiscutellum herwigorum n. gen., n. sp. (Trilobita) from the Upper Honsel Beds of the north-western Sauerland (Lower Givetian, Rhenohercynian Zone), with a contribution to scutelluid systematic, Neues Jahrb. Geol. Paläontol., 281, 51–93, https://doi.org/10.1127/njgpa/2016/0587, 2016.

Becker, R., Aboussalam, Z., Stichling, S., and May, A.: The Givetian-Frasnian Hönne Valley Reef Complex (northern Sauerland) – an outline of stratigraphy and facies development, Münster. Forsch. Geol. Paläont., 108, 126–140, 2016.

Böhm, F., Koch, R., Höferle, R., and Baasch, R.: Der Malm in der Geothermiebohrung Pullach Th2 - Faziesanalyse aus Spülproben (München, S-Deutschland), Geol. Bl. NO-Bayern, 60, 17–49, 2010.

Bonnet, E., Bour, O., Odling, N. E., Davy, P., Main, I., Cowie, P., and Berkowitz, B.: Scaling of fracture systems in geological media, Rev. Geophys., 39, 347–383, https://doi.org/10.1029/1999RG000074, 2001.

Brix, M. R., Drozdzewski, G., Greiling, R. O., Wolf, R., and Wrede, V.: The N Variscan margin of the Ruhr coal district (Western Germany): structural style of a buried thrust front?, Geol. Rundsch., 77, 115–126, https://doi.org/10.1007/BF01848679, 1988.

Brown, S. R.: Fluid flow through rock joints: the effect of surface roughness, J. Geophys. Res. - Sol. Ea., 92, 1337–1347, https://doi.org/10.1029/JB092iB02p01337, 1987.

Brudy, M., Zoback, M. D., Fuchs, K., Rummel, F., and Baumgärtner, J.: Estimation of the complete stress tensor to 8 km depth in the KTB scientific drill holes: Implications for crustal strength, J. Geophys. Res. - Sol. Ea., 102, 18 453–18 475, https://doi.org/10.1029/96JB02942, 1997.

Cappa, F., Guglielmi, Y., Fénart, P., Merrien-Soukatchoff, V., and Thoraval, A.: Hydromechanical interactions in a fractured carbonate reservoir inferred from hydraulic and mechanical measurements, Int. J. Rock Mech. Min., 42, 287–306, https://doi.org/10.1016/j.ijrmms.2004.11.006, 2005.

Čermák, V. and Rybach, L.: Thermal conductivity and specific heat of minerals and rocks, in: Landolt-Börnstein: Numerical Data and Functional Relationships in Science and Technology, New Series, Group V (Geophysics and Space Research), Volume Ia (Physical Properties of Rocks), edited by Angenheister, G., pp. 305–343, Springer, Berlin-Heidelberg, 1982.

Clauser, C. and Huenges, E.: Thermal Conductivity of Rocks and Minerals, in: Rock Physics & Phase Relations, edited by Ahrens, T. J., pp. 105–126, American Geophysical Union (AGU), https://doi.org/10.1029/RF003p0105, 2013.

Cruden, D.: Describing the size of discontinuities, Int. J. Rock Mech. Min., 14, 133–137, https://doi.org/10.1016/0148-9062(77)90004-3, 1977.

Da Prat, G.: Well test analysis for fractured reservoir evaluation, Elsevier, 1990.

Dahi Taleghani, A. and Olson, J. E.: How natural fractures could affect hydraulic-fracture geometry, SPE Journal, 19, 161–171, https://doi.org/10.2118/167608-PA, 2013.

Dallmeyer, R. D., Franke, W., and Weber, K.: Pre-Permian geology of central and eastern Europe, Springer Science & Business Media, Berlin, Heidelberg, 2013.

Darcy, H. P. G.: Les Fontaines publiques de la ville de Dijon. Exposition et application des principes à suivre et des formules à employer dans les questions de distribution d'eau, etc, V. Dalmont, Paris, 1856.

DEKORP Research Group: Results of deep-seismic reflection investigations in the Rhenish Massif, Tectonophysics, 173, 507–515, https://doi.org/10.1016/0040-1951(90)90242-Z, 1990.

Der Kiureghian, A. and Ditlevsen, O.: Aleatory or epistemic? Does it matter?, Struct. Saf., 31, 105–112, https://doi.org/10.1016/j.strusafe.2008.06.020, 2009.

DIN 18124: Determination of density of solid particles – Capillary pyknometer, wide mouth pycnometer, gas pycnometer, 2011.

Drozdzewski, G.: Beiträge zur Tiefentektonik westdeutscher Steinkohlenlagerstätten, Geolog. Landesamt Nordrhein-Westfalen, Krefeld, 1985.

Drozdzewski, G. and Wrede, V.: Faltung und Bruchtektonik – Analyse der Tektonik im Subvariscikum, Fortschritte in der Geologie von Rheinland und Westfalen, 38, 7–187, 1994.

Drozdzewski, G., Grabert, H., Hartkop-Fröder, C., Jansen, F., Juch, D., Pieper, B., Schlimm, W., Stehn, O., Steuerwald, K., Suchan, K.-H., Thome, K., and Vogler, H.: Erläuterungen zur Geologischen Karte von Nordrhein-Westfalen 1:100 000, Blatt C 4706 Düsseldorf - Essen, Geolog. Landesamt Nordrhein-Westfalen, Krefeld, 2007.

Duda, M. and Renner, J.: The weakening effect of water on the brittle failure strength of sandstone, Geophys. J. Int., 192, 1091–1108, https://doi.org/10.1093/gji/ggs090, 2013.

Engel, W., Franke, W., and Langenstrassen, F.: Palaeozoic sedimentation in the northern branch of the mid-European Variscides — Essay of an interpretation, in: Intracontinental fold belts, pp. 9–41, Springer, Berlin, Heidelberg, https://doi.org/10.1007/978-3-642-69124-9_2, 1983.

Evans, J. P., Forster, C. B., and Goddard, J. V.: Permeability of fault-related rocks, and implications for hydraulic structure of fault zones, J. Struct. Geol., 19, 1393–1404, https://doi.org/10.1016/S0191-8141(97)00057-6, 1997.

Far, M. E.: Seismic characterization of naturally fractured reservoirs, Dissertation, University of Houston, 2011.

Flügel, E. and Hötzl, H.: Palökologische und statistische Untersuchungen in mitteldevonischen Schelf-Kalken (Schwelmer Kalk, Givet; Rheinisches Schiefergebirge), Bayerische Akad. Wiss., München, 1976.

Franke, W. and Engel, W.: Variscan sedimentary basins on the Continent, and relations with south-west England, Proc. Ussher., 5, 259–269, 1982.

Franke, W., Bortfeld, R. K., Brix, M., Drozdzewski, G., Dürbaum, H. J., Giese, P., Janoth, W., Jödicke, H., Reichert, C., Scherp, A., Schmoll, J., Thomas, R., Thünker, M., Weber, K., Wiesner, M. G., and Wong, H. K.: Crustal structure of the Rhenish Massif: results of deep seismic reflection lines Dekorp 2-North and 2-North-Q, Geol. Rundsch., 79, 523–566, https://doi.org/10.1007/BF01879201, 1990.

Franke, W., Cocks, L. R. M., and Torsvik, T. H.: The Palaeozoic Variscan oceans revisited, Gondwana Res., 48, 257–284, https://doi.org/10.1016/j.gr.2017.03.005, 2017.

Fridleifsson, I. B., Bertani, R., Huenges, E., Lund, J. W., Ragnarsson, A., and Rybach, L.: The possible role and contribution of geothermal energy to the mitigation of climate change, in: IPCC scoping meeting on renewable energy sources, proceedings, Luebeck, Germany, vol. 20, pp. 59–80, Citeseer, https://doi.org/20.500.11850/13474, 2008.

Fritzer, T., Settles, E., and Dorsch, K.: Bayerischer Geothermieatlas – Hydrothermale Energiegewinnung, Bayerisches Staatsministerium für Wirtschaft, Infrastruktur, Verkehr und Technologie, Munich, Germany (in German), 2010.

Ganoulis, J.: Engineering risk analysis of water pollution: probabilities and fuzzy sets, John Wiley & Sons, Weinheim, 2008.

Gassmann, F.: Über die elastizität poröser medien: Vier. der Natur, Gesellschaft Zürich, 96, 1–23, 1951.

Gebrande, H.: 3.1.3 Elastic wave velocities and constants of elasticity of rocks at room temperature and pressures < 1 GPa: Datasheet from Landolt-Börnstein - Group V Geophysics · Volume 1B, in: Subvolume B, edited by Angenheister, G., pp. 35–38, Springer-Verlag Berlin Heidelberg, https://doi.org/10.1007/10201909_7, 1982.

Gillhaus, A., GÖtte, T., and Richter, D. K.: Polyphase spätdiagenetische Dolomitbildung im mittel-bis oberdevonischen Massenkalk von Hagen-Hohenlimburg (Remscheid-Altenaer Sattel, Rheinisches Schiefergebirge), Mitt. Ges. Geol. Bergbaustud. Österr, 46, 51–66, 2003.

Goldstein, B., Hiriart, G., Tester, J., Bertani, B., Bromley, R., Gutierrez-Negrin, L., Huenges, E., Ragnarsson, A., Mongillo, A., Muraoka, H., and Zui, V. I.: Great expectations for geothermal energy to 2100, in: Proceedings 36th Workshop on Geothermal Reservoir Engineering, 2011.

Grabert, H.: Abriß der Geologie von Nordrhein-Westfalen, Schweizerbart'sche Verlagsbuchhandlung, Stuttgart, 1998.

Guerriero, V., Mazzoli, S., Iannace, A., Vitale, S., Carravetta, A., and Strauss, C.: A permeability model for naturally fractured carbonate reservoirs, Mar. Petrol. Geol., 40, 115–134, https://doi.org/10.1016/j.marpetgeo.2012.11.002, 2013.

Hancock, P. L. and Bevan, T. G.: Brittle modes of foreland extension, Geol. Soc. Spec. Publ., 28, 127–137, https://doi.org/10.1144/GSL.SP.1987.028.01.10, 1987.

Hashin, Z. and Shtrikman, S.: A variational approach to the theory of the elastic behaviour of multiphase materials, J. Mech. Phys. Solids, 11, 127–140, https://doi.org/10.1016/0022-5096(63)90060-7, 1963.

Heidbach, O., Rajabi, M., Reiter, K., Ziegler, M., et al.: World stress map database release 2016, GFZ Data Services, https://doi.org/10.5880/WSM.2016.002, 2016.

Hesemann, J.: Die Ergebnisse der Bohrung Münsterland 1, Springer Fachmedien Wiesbaden, 1965.

Hirschberg, S., Wiemer, S., and Burgherr, P.: Energy from the Earth. Deep Geothermal as Resource for the Future?, vdf Hochschulverlag AG, Zurich, Switzerland, 2015.

Hoek, E. and Brown, E.: Practical estimates of rock mass strength, Int. J. Rock Mech. Min., 34, 1165–1186, https://doi.org/10.1016/S1365-1609(97)80069-X, 1997.

Holder, M. T. and Leversidge, B. E.: A model for the tectonic evolution of south Cornwall, J. Geol. Soc. London, 143, 125–134, https://doi.org/10.1144/gsjgs.143.1.0125, 1986.

Homuth, S.: Aufschlussanalogstudie zur Charakterisierung oberjurassischer geothermischer Karbonatreservoire im Molassebecken, Dissertation, Technische Universität Darmstadt, 2014.

Homuth, S., Götz, A. E., and Sass, I.: Reservoir characterization of the Upper Jurassic geothermal target formations (Molasse Basin, Germany): role of thermofacies as exploration tool, Geoth. Energ. Sci., 3, 41–49, https://doi.org/10.5194/gtes-3-41-2015, 2015a.

Homuth, S., Götz, A., and Sass, I.: Physical Properties of the Geothermal Carbonate Reservoirs of the Molasse Basin, Germany - Outcrop Analogue vs. Reservoir Data, 2015b.

Hudson, J. A.: Engineering Properties of Rocks, Elsevier, 2005.

ISRM: International society for rock mechanics commission on standardization of laboratory and field tests: Suggested methods for the quantitative description of discontinuities in rock masses, Int. J. Rock Mech. Min., 15, 319–368, https://doi.org/10.1016/0148-9062(78)91472-9, 1978.

Jansen, F., von Kamp, H., Kühn-Velten, H., Kunz, E., Müller, H., Paproth, E., Rabitz, A., Thome, K., and Vogler, H.: Erläuterung zur Geologische Karte von Nordrhein-Westfalen 1: 100 000, Blatt C 4710 Dortmund, Geolog. Landesamt Nordrhein-Westfalen, Krefeld, 1986.

Jorand, R., Clauser, C., Marquart, G., and Pechnig, R.: Statistically reliable petrophysical properties of potential reservoir rocks for geothermal energy use and their relation to lithostratigraphy and rock composition: The NE Rhenish Massif and the Lower Rhine Embayment (Germany), Geothermics, 53, 413–428, https://doi.org/10.1016/j.geothermics.2014.08.008, 2015.

Jux, U.: Die devonischen Riffe im rheinischen Schiefergebirge, Teile I und II, vol. 110, N. Jb. Geol. u. Paläont., Stuttgart, 1960.

Kelley, V. C. and Clinton, N. J.: Fracture systems and tectonic elements of the Colorado Plateau, 6-7, University of New Mexico Press, 1960.

Klaus, T., Vollmer, C., Werner, K., Lehmann, H., and Müschen, K.: Energieziel 2050: 100% Strom aus erneuerbaren Quellen, Dessau: Umweltbundesamt, 2010.

Kley, J.: Saxonische Tektonik im 21. Jahrhundert, Z. Dtsch. Ges. Geowiss., 164, 295–311, https://doi.org/10.1127/1860-1804/2013/0022, 2013.

Kloke, R.: Geologische Kartierung des Steinbruchgebietes Asbeck, Hönnetal (NRW), Dissertation, Ruhr-Universität Bochum, 2007.

Knutzen, L. K.: Geothermal and spatial coupled site selection for the connection of deep geothermal plants to existing district heating networks on the example of the Ruhr Metropolitan Region, Dissertation, Ruhr-Universität Bochum, 2017.

Koch, L.: Aus Devon, Karbon und Kreide: die fossile Welt des nordwestlichen Sauerlandes, Hagen v. d. Linnepe, 1984.

Koch-Früchtel, U. and Früchtel, M.: Stratigraphie und Faziesanalyse einer mitteldevonischen arbonatabfolge im Remscheid-Altenaer Sattel (Sauerland), Geol. Paläont. Westf., 26, 47–75, 1993.

Kossmat, F.: Gliederung des varistischen Gebirgsbaues, Abh. Sächisches Geol. Landesamtes, 1, 1–39, 1927.

Kranz, R. L., Frankel, A. D., Engelder, T., and Scholz, C. H.: The permeability of whole and jointed Barre Granite, Int. J. Rock. Mech. Min., 16, 225–234, https://doi.org/10.1016/0148-9062(79)91197-5, 1979.

Krebs, W.: Reef development in the Devonian of the eastern Rhenish Slate Mountains, Germany, CSPG Spec. Pub., 2, 295–306, 1967.

Krebs, W.: Devonian Carbonate Complexes of Central Europe, AAPG Bull., 54, 856–857, https://doi.org/10.1306/5D25CAE9-16C1-11D7-8645000102C1865D, 1970.

La Pointe, P. R. and Hudson, J. A.: Characterization and interpretation of rock mass joint patterns, Geological Society of America, Wisconsin, 1985.

Lacazette, A.: A new stereographic technique for the reduction of scanline survey data of geologic fractures, Comput. Geosci., 17, 445–463, https://doi.org/10.1016/0098-3004(91)90051-E, 1991.

Laubach, S. E., Olson, J. E., and Gale, J. F. W.: Are open fractures necessarily aligned with maximum horizontal stress?, Earth Planet. Sc. Lett., 222, 191–195, 2004.

Littke, R., Bayer, U., Gajewski, D., and Nelskamp, S.: Dynamics of complex intracontinental basins: the central European basin system, Springer Science & Business Media, Berlin, Heidelberg, 2008.

Lorenz, J. C., Teufel, L. W., and Warpinski, N. R.: Regional Fractures I: A Mechanism for the Formation of Regional Fractures at Depth in Flat-Lying Reservoirs1, AAPG Bull., 75, 1714–1737, https://doi.org/10.1306/0C9B29E3-1710-11D7-8645000102C1865D, 1991.

Lucia, J. F., Charles, K., and James, J.: Carbonate Reservoir Characterization, vol. 2, Springer, Berlin, Heidelberg, https://doi.org/10.1007/978-3-540-72742-2, 2007.

Markovaara-Koivisto, M. and Laine, E.: MATLAB script for analyzing and visualizing scanline data, Comput. Geosci., 40, 185–193, https://doi.org/10.1016/j.cageo.2011.07.010, 2012.

MATLAB: version 9.4.0. (R2018a), The MathWorks Inc., Natick, Massachusetts, 2018.

Mavko, G., Mukerji, T., and Dvorkin, J.: The Rock Physics Handbook, Cambridge University Press, Cambridge, 3 edn., https://doi.org/10.1017/CBO9780511626753, 2020.

Meschede, M.: Deutschland im späten Paläozoikum, in: Geologie Deutschlands, pp. 61–101, Springer, Berlin, Heidelberg, 2 edn., https://doi.org/10.1007/978-3-662-56422-6, 2018.

Narr, W.: Fracture Density in the Deep Subsurface: Techniques with Application to Point Arguello Oil Field, AAPG Bull., 75, 1300–1323, https://doi.org/10.1306/0C9B2939-1710-11D7-8645000102C1865D, 1991.

Narr, W.: Estimating Average Fracture Spacing in Subsurface Rock, AAPG Bull., 80, 1565–1585, https://doi.org/10.1306/64EDA0B4-1724-11D7-8645000102C1865D, 1996.

Nelson, R.: Geologic analysis of naturally fractured reservoirs, Elsevier, 2001.

Nelson, R. A. and Handin, J.: Experimental study of fracture permeability in porous rock, AAPG Bull., 61, 227–236, https://doi.org/10.1306/C1EA3C2B-16C9-11D7-8645000102C1865D, 1977.

Nickelsen, R. P. and Hough, V. N. D.: Jointing in the Appalachian Plateau of Pennsylvania, AAPG Bull., 78, 609–630, https://doi.org/10.1130/0016-7606(1967)78[609:JITAPO]2.0.CO;2, 1967.

Odling, N. E., Gillespie, P., Bourgine, B., Castaing, C., Chiles, J. P., Christensen, N. P., Fillion, E., Genter, A., Olsen, C., Thrane, L., Trice, R., Aarseth, E., Walsh, J. J., and Watterson, J.: Variations in fracture system geometry and their implications for fluid flow in fractures hydrocarbon reservoirs, Petrol. Geosci., 5, 373–384, https://doi.org/10.1144/petgeo.5.4.373, 1999.

Oncken, O.: Transformation of a magmatic arc and an orogenic root during oblique collision and it's consequences for the evolution of the European Variscides (Mid-German Crystalline Rise), Geol. Rundsch., 86, 2–20, https://doi.org/10.1007/s005310050118, 1997.

Ozkaya, S. I.: A Simple Formula To Estimate 2D Fracture Connectivity, SPE Reservoir Evaluation & Engineering, 14, 763–775, 2011.

Paeckelmann, W.: Erläuterungen zur Geologische Karte von Preußen und benachbarten deutschen Ländern, Blatt Balve, Geolog. Landesamt Nordrhein-Westfalen, Krefeld, 1938.

Paeckelmann, W.: Erläuterungen zur Geologischen Karte von Nordrhein-Westfalen 1:25000, Blatt 4708 Wuppertal-Elberfeld, Geolog. Landesamt Nordrhein-Westfalen, Krefeld, 1979.

Paeckelmann, W. and Zimmermann, E.: Erläuterungen zur Geologischen Karte von Preußen und benachbarten deutschen Ländern, Blatt Mettmann, Geolog. Landesamt Nordrhein-Westfalen, Krefeld, 1930.

Pas, D., Da Silva, A.-C., Cornet, P., Bultynck, P., Königshof, P., and Boulvain, F.: Sedimentary development of a continuous Middle Devonian to Mississippian section from the fore-reef fringe of the Brilon Reef Complex (Rheinisches Schiefergebirge, Germany), Facies, 59, 969–990, https://doi.org/10.1007/s10347-012-0351-z, 2013.

Paterson, M. S. and Wong, T.-F.: Experimental Rock Deformation – The Brittle Field, Springer Science & Business Media, Berlin, Heidelberg, New York, 2005.

Popov, Y. A.: Optical scanning technology for nondestructive contactless measurements of thermal conductivity and diffusivity of solid matters, Exp. Heat Transfer, Fluid Mech. Thermodyn., 1, 109–117, 1997.

Priest, S. D.: Discontinuity Analysis for Rock Engineering, Springer Science & Business Media, London; New York, https://doi.org/10.1007/978-94-011-1498-1, 1995.

Priest, S. D. and Hudson, J. A.: Discontinuity spacings in rock, Int. J. Rock. Mech. Min., 13, 135–148, https://doi.org/10.1016/0148-9062(76)90818-4, 1976.

Priest, S. D. and Hudson, J. A.: Estimation of discontinuity spacing and trace length using scanline surveys, Int. J. Rock Mech. Min., 18, 183–197, https://doi.org/10.1016/0148-9062(81)90973-6, 1981.

Roberts, J. C.: Jointing and minor tectonics of the Vale of Glamorgan between Ogmore-By-Sea and Lavernock Point, South Wales, Geol. J., 9, 97–114, https://doi.org/10.1002/gj.3350090201, 1974.

Rummel, F. and Weber, U.: Stress field in the coal mines of the Ruhr coal district, in: The 34th US Symposium on Rock Mechanics (USRMS), ARMA, 1993.

Salamon, M. and Königshof, P.: Middle Devonian olistostromes in the Rheno-Hercynian zone (Rheinisches Schiefergebirge) – An indication of back arc rifting on the southern shelf of Laurussia, Gondwana Res., 17, 281–291, https://doi.org/10.1016/j.gr.2009.10.004, 2010.

Santos, R. F. V. C., Miranda, T. S., Barbosa, J. A., Gomes, I. F., Matos, G. C., Gale, J. F. W., Neumann, V. H. L. M., and Guimarães, L. J. N.: Characterization of natural fracture systems: Analysis of uncertainty effects in linear scanline results, AAPG Bull., 99, 2203–2219, https://doi.org/10.1306/05211514104, 2015.

Scheck-Wenderoth, M., Krzywiec, P., Zühlke, R., Maystrenko, Y., and Froitzheim, N.: Permian to Cretaceous tectonics, in: The Geology of Central Europe: Mesozoic and Cenozoic, edited by McCann, T., vol. 2, pp. 999–1030, The Geological Society London, London, 2008.

Scheer, D., Konrad, W., and Scheel, O.: Public evaluation of electricity technologies and future low-carbon portfolios in Germany and the USA, Energ. Sustain. Soc., 3, 8, https://doi.org/10.1186/2192-0567-3-8, 2013.

Schellschmidt, R., Sanner, B., Pester, S., and Schulz, R.: Geothermal energy use in Germany, in: Proceedings World Geothermal Congress, vol. 152, p. 19, 2010.

Schudack, M.: Karbonatzyklen in Riff- und Lagunenbereichen des devonischen Massenkalkkomplexes von Asbeck (Hönnetal, Rheinisches Schiefergebirge), Geol. Paläont. Westf., 26, 77–106, 1993.

Stearns, D. W. and Friedman, M.: Stratigraphic Oil and Gas Fields – Classification, Exploration Methods, and Case Histories, in: Reservoirs in Fractured Rock, American Association of Petroleum Geologists, https://doi.org/10.1306/M16371C8, 1972.

Stober, I.: Hydrochemical properties of deep carbonate aquifers in the SW German Molasse basin, Geothermal Energy, 2, 13, https://doi.org/10.1186/s40517-014-0013-1, 2014.

Terzaghi, R. D.: Sources of Error in Joint Surveys, Geotechnique, 15, 287–304, https://doi.org/10.1680/geot.1965.15.3.287, 1965.

van Golf-Racht, T. D.: Fundamentals of fractured reservoir engineering, Elsevier, 1982.

von Kamp, H. and Ribbert, K. H.: Erläuterungen zur Geologischen Karte von Nordrhein-Westfalen 1:25000, Blatt 4611 Hagen-Hohenlimburg, Geolog. Landesamt Nordrhein-Westfalen, Krefeld, 2005.

Wagner, W.: FLUIDCAL, software for calculation of thermodynamic properties for a great number of substances, F.I.R.S.T. – Gesellschaft für technisch-wissenschaftliche Softwareanwendungen mbH, Wermelskirchen, 2009.

Watkins, H., Bond, C. E., Healy, D., and Butler, R. W.: Appraisal of fracture sampling methods and a new workflow to characterise heterogeneous fracture networks at outcrop, J. Struct. Geol., 72, 67–82, 2015.

Wegener, M., Schwarze, B., Spiekermann, K., Brosch, K., Huber, F., Müller, M., and Reutter, O.: Modelling the great transformation in the Ruhr area, Transp. Res. Proc., 41, 231–239, https://doi.org/10.1016/j.trpro.2019.09.042, 2019.

Wilson, C. E., Aydin, A., Karimi-Fard, M., Durlofsky, L. J., Amir, S., Brodsky, E. E., Kreylos, O., and Kellogg, L. H.: From outcrop to flow simulation: Constructing discrete fracture models from a LIDAR survey, AAPG Bull., 95, 1883–1905, https://doi.org/10.1306/03241108148, 2011.

Ziegler, P. A.: Geological Atlas of Western and Central Europe, Shell Int. Petr. Mij, The Hague, Netherlands, 2 edn., 1990.